Journal Pre-proof

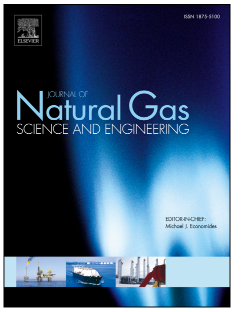


# A Fracture Upscaling Method (FUM) for Hydraulically Fractured Reservoirs: from Discrete Fracture Modelling to Finite Difference Simulations

Joseph Sherratt, Amin Sharifi Haddad, Roozbeh Rafati, Mehrdad T. Manzari

PII: S1875-5100(20)30465-0

DOI: https://doi.org/10.1016/j.jngse.2020.103611

Reference: JNGSE 103611

To appear in: *Journal of Natural Gas Science and Engineering*

Received Date: 14 April 2020

Revised Date: 28 August 2020

Accepted Date: 4 September 2020

Please cite this article as: Sherratt, J., Haddad, A.S., Rafati, R., Manzari, M.T., A Fracture Upscaling Method (FUM) for Hydraulically Fractured Reservoirs: from Discrete Fracture Modelling to Finite Difference Simulations, *Journal of Natural Gas Science & Engineering*, https://doi.org/10.1016/j.jngse.2020.103611.

This is a PDF file of an article that has undergone enhancements after acceptance, such as the addition of a cover page and metadata, and formatting for readability, but it is not yet the definitive version of record. This version will undergo additional copyediting, typesetting and review before it is published in its final form, but we are providing this version to give early visibility of the article. Please note that, during the production process, errors may be discovered which could affect the content, and all legal disclaimers that apply to the journal pertain.

© 2020 Elsevier B.V. All rights reserved.

**Joseph Sherratt:** Conceptualization, Methodology, Software, Validation, Writing - Original Draft. **Amin Sharifi Haddad:** Conceptualization, Supervision, Formal analysis, Writing - Review & Editing. **Roozbeh Rafati**: Supervision, Validation. **Mehrdad T Manzari***:* Supervision, Writing - Review & Editing.

Journal Pre-proof

Journal Pre-proof

# A Fracture Upscaling Method (FUM) for Hydraulically Fractured Reservoirs: from Discrete Fracture Modelling to Finite Difference Simulations

Joseph Sherratt[1], Amin Sharifi Haddad[1*], Roozbeh Rafati[1], Mehrdad T. Manzari[2]

[1]School of Engineering, University of Aberdeen, King's College, Aberdeen, UK, AB24 3UE

[2] School of Geosciences, University of Aberdeen, King's College, Aberdeen, UK, AB24 3UE

**Abstract**

Hydraulic fracturing creates a complex fracture geometry in heterogeneous formations which are frequently simulated using Finite Element based fracture propagation modelling tools. Representing this geometry in Finite Difference based multiphase flow simulators poses some challenges. In this study, a Fracture Upscaling Method (FUM) is developed to represent complex fracture systems generated by the finite element method. It is demonstrated that this method can capture complex fracture geometries even when using coarse grids. This upscaling method can be used as a coupling tool between the output of any discrete fracture model and any finite difference-based reservoir simulator. FUM is tested against a field case and simulation results show a reasonable match with 120 days of production data. This method is then used to investigate the impact that natural fractures have on production from shale gas wells. The results show that the effect of orientation, spacing and length of natural fractures, on propagating hydraulic fractures can reduce the recovery factor by 30%. Furthermore, the ability of FUM to combine highly complex fracture networks with realistic multiple layer models with complex distributions of reservoir properties is demonstrated.

**Keywords:** Hydraulic fracturing, Fracture patterns, Upscaling, Finite difference simulations, Discrete fracture models

## 1. Introduction

The development of horizontal drilling and hydraulic fracturing process have unlocked large volumes of previously inaccessible hydrocarbons. This has had the largest impact in the US

Journal Pre-proof

which produces 11 million barrels of oil per day of which over 7 million barrels are from shale (EIA, 2019). Similarly, shale gas production is now 50 billion cubic feet per day in the US, which is over 50% of its total gas production (EIA, 2018). Shale gas also represents 62% of total proven gas reserves in the US (U.S. Department of Energy, 2018), and it has the potential to reduce global $CO_2$ emissions to half by replacing coal electricity generation with gas (Liang et al., 2012, Burnham et al., 2012).

Recovery from tight reservoirs is still very low with oil recovery typically being 5-10% of original oil in place (OOIP) and gas recovery is typically up to 35%, although this decreases with geological complexity (Godec et al., 2013, Egboga, Mohanty & Balhoff, 2017). Coupled with the high cost of fracturing process, there is a need to increase the recovery from hydraulically fractured formations. The success of stimulation relies on connecting large volumes of the reservoir with the well. Through a better understanding and ability to model the process, it is hoped that well placement and design can be optimised so that this recovery is maximised.

Shale permeability is in the range of 70 to 500 nanodarcies (Fisher et al, 2004). Through the injection of a mixture of water and proppants at high pressures, hydraulic fractures are created to connect the formation to the well. Classical rock/fracture mechanics suggests that hydraulic fractures will open in the least energy configuration, i.e., fractures propagate perpendicular to the least in-situ principal stress. Wells are therefore drilled parallel to the least principal stress so that fractures propagate deep into the target formation away from the well and ensure maximum productivity. Microseismic events suggest that more complex fracture networks are produced which are not conformable with classical mechanics (Daniels et al., 2007). The complexity has been explained by two main mechanisms; heterogeneity of the formation (e.g., existence of different facies and natural fractures) and stress shadow effects (Kresse et al., 2012, Kresse et al., 2013). Hydraulic fractures exploit planes of weakness, such as natural fractures, resulting in complex fracture networks with lots of branches. Previous studies on the effect of reservoir properties on fracture propagation have shown that high differential stresses decrease fracture length and increase the complexity of fracture geometry (Wu & Olson, 2015, Liu et al., 2018). In addition to this a phenomenon referred to as the stress shadow has been shown to be able to rotate the direction of propagation of fractures up to 90° so that they may intersect other fractures from previous stages (Roussel & Sharma, 2011).

Finite Element Modelling captures the propagation of fractures by representing the fractures using discrete elements (Kresse et al., 2012, Kresse et al., 2013). This is the most successful approach to analyse the complex interactions between propagating hydraulic fractures in heterogeneous formations. These simulations are often dynamic; allowing for the effect of fluid leak off and proppant transport to be incorporated.

Once the hydraulic fracture patterns are created considering geomechanics of the subsurface environment, then modelling oil and gas production from hydraulically fractured reservoirs can be conducted using several different methods. In most of the multiphase flow calculations (e.g., reservoir simulators), the hydraulic fractures are often represented as simple discontinuities, and hence in these calculations complex fracture geometries are not captured. Therefore, in conventional simulators the fracture is often treated as a linear set of cells with high permeability (Moreno et al., 2014). An excessive simplification of fracture geometry can seriously impact the accuracy of these models. Complex hydraulic fracture networks can be modelled using the Stimulated Reservoir Volume (SRV) method (Ren et al., 2018). The mechanically failed region is described as a zone of enhanced permeability instead of a discrete object, taking into account complex interactions such as shear fracturing (Nassir et al., 2010, Nassir et al., 2014). The SRV method can easily model fluid production as each cell already has an altered permeability but has the same issue that fails to capture the complex geometry of fractures. Semi-implicit models have also been developed to calculate production from complex fracture networks by representing the network as combination of fracture units (Luo et al., 2019). This can capture the complexity of fracture networks but assumes petrophysical properties such as reservoir permeability are constant across the reservoir.

Embedded discrete fracture models (EDFM) also called discrete fracture models (DFM) use a multiple porosity approach to include cells containing conductive planes (Moinfar et al., 2014). In this type of modelling, cells are divided into multiple regions allowing for complex transfer between matrix, organic material and fractures to occur. Discrete fracture modelling has also been used to determine hydrological behaviour of fractured rocks on a smaller scale (Lei et al., 2017). This method has also been coupled with other techniques such as moving tip clustering and linear regression clustering to capture even more complex branches of microcracks (Wan et al., 2020). Therefore, DFMs capture the complexity of fracture networks but are computationally expensive and require the development of unique stand-alone software.

Furthermore, accurate representation of fracture network and its upscaling model are necessary to predict the performance of enhanced gas or oil recovery processes in hydraulically fractured reservoir. In previous studies it was shown that the size and shape of the matrix and fracture are important to design an optimised recovery process from fractured rocks, therefore simplifying the hydraulic fractures with a simple set of high permeability cells in reservoir simulations may cause inaccuracies in the production (Sharifi Haddad et al. 2012, Sharifi Haddad et al. 2013, Sharifi Haddad et al. 2017, Sherratt et al. 2018). Existing software can capture many of these complex phenomena but are unable to incorporate DFMs as they use finite-difference methods.

To summarise, Finite Element Methods excel at capturing fracture propagation but utilising this complex fracture geometry in flow simulators is a challenge. In the past, this has either been approached by reducing the complexity or with the development of specialist software, but is there a simpler approach?

In this study we propose a fracture upscaling method that uses the output of geomechanics simulators (based on Finite Element Methods) to create complex fracture networks to be used in connection with finite difference numerical simulators. This approach is referred to as the fracture upscaling model (FUM). By utilising FUM, through a fracture upscaling method, production from complex hydraulic fracture networks can be computed using a conventional reservoir simulator. A simplified approach for modelling fractures in computational grids has been used to represent non-planar fractures, where the fracture properties such as aperture and height were assumed to be constant along the fracture (Sakhaee-Pour & Wheeler, 2016). We introduce an extended method for the upscaling of fractures by incorporating the complex output of fracture propagation models. Furthermore, to be able to apply the model to real scenarios we considered variation of fracture properties in our model, hence, in FUM a distribution of fracture properties can be incorporated.

Past studies have investigated the impact of reservoir properties and stimulation parameters on the propagation of fractures into the formation using FEM approaches (Kresse et al., 2012, Kresse et al., 2013). In this study, by using FUM, we determine how production from such hydraulically fractured reservoirs is impacted by these properties considering the resulted hydraulic fractures propagation. This should help to identify scenarios that are favourable and those which can be easily excluded.

FUM still results in some simplification of fracture geometry in comparison with DFM. But it can simplify the problem by not requiring a specially designed reservoir simulator. By



Journal Pre-proof

coupling DFMs with commonly used Finite-Difference based reservoir simulators FUM also provides an opportunity to conduct complex multiphase flow simulations for enhanced recovery processes in hydraulically fractured tight formations. However, fine grids are required to ensure the simplification is limited which can increase computational time and expense.

## 2. Methodology

This study presents a method of upscaling discrete fracture networks to a finite difference-based computational grid so that multiphase flow in hydraulically fractured reservoirs can be modelled using a conventional reservoir simulator. In the developed FUM algorithm, a geological model is the first input that is used by a discrete fracture network (DFN) simulation software. The same geological model is also used to create a finite-difference based computational grid. Depending on the complexity of the geological structure of the formation, highly complex 3D grids may be created. However, in this study, for simplicity of the demonstration of FUM, we combine complex 3D fracture propagation results with a simple single layer thick reservoir grid. FUM is developed in C++ to combine and upscale the discrete fracture network with a dual-permeability finite difference-based reservoir grid. The general algorithm developed in this study is shown in Figure 1.

Journal Pre-proof

Journal Pre-proof

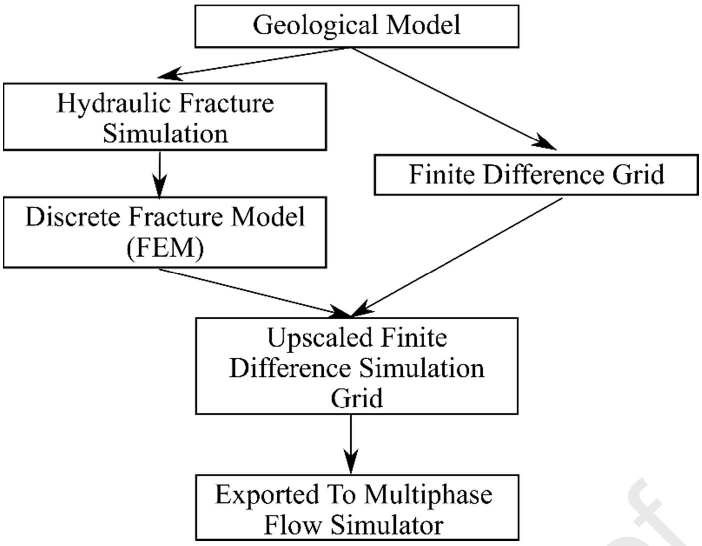


*Figure 1 – Flow diagram of the upscaling method developed in this study*

Before production is modelled, the hydraulic fracture network is generated by a commercially available unconventional fracture modelling software which is able to capture the complexity of interactions with natural fractures and stress shadow effects (Kresse et al., 2013). The fracture propagation is modelled using a volumetric approach to determine pressure distribution within the fracture network and failure criteria are evaluated to determine if and how the fracture propagates. Many parameters can affect the propagation of fractures including the principal stresses, Young's modulus and intrinsic matrix permeability. The resulting fracture networks have both complex geometry and complex distribution of properties such as aperture which must be considered when calculating the ability of the fracture network to conduct flow at each point in the network. The developed fractures need to be coupled with multiphase flow solvers. FUM is developed as a framework which can be applied to any discrete fracture network to be upscaled and used to simulate production in any finite-difference based multiphase flow simulator.

DFNs describe the fracture network as thousands of surfaces which are also referred to as patches. Patches are usually triangular as all vertices of a triangle always lie on a common plane. The fracture properties such as aperture and proppant concentration are also defined at

Journal Pre-proof

each vertex on each surface. The common plane that all three corner points lie on, specify the orientation of the fracture, and the edges of the surface define the boundaries of the fracture. A conventional reservoir simulator represents the reservoir as a set of individual cells and each cell is assigned the average properties of the volume it represents. In this study FUM is only applied to simple cuboidal cells but could be expanded to incorporate more complex grid geometries.

To determine the effect that the hydraulic fracture has on a cell, the intersection of each fracture with that cell must be found as shown in Figure 2 (a). This shows eight individual patches that all correspond to a single fracture surface and are all contained within a single cell. This is a computationally expensive process as each triangular patch must be compared with each computational cell to determine if there is any intersection. If there is an intersection i.e. the patch is only partially contained within the cell, then that part of the triangular element contained within the cell must be found. A cell may also contain many patches, or parts of patches, that all correspond to the same fracture plane. With highly complex fracture systems a single cell may also contain fracture patches corresponding to multiple fracture planes as shown in Figure 2 (b).

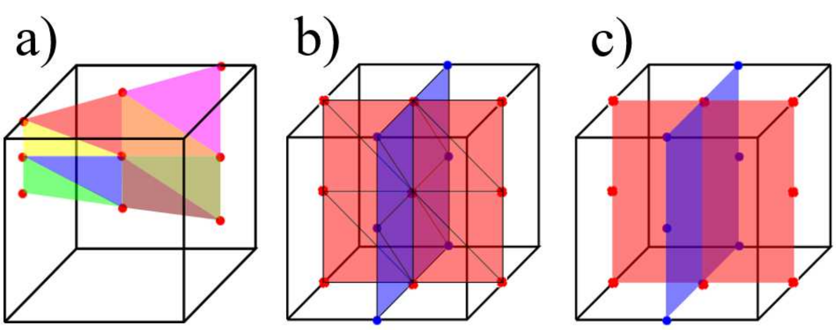


*Figure 2 – An example of a) how triangular fracture patches defining a single fracture plane are contained within a single cell, b) a single cell containing multiple fracture patches corresponding to two different fractures and c) the resulting contained fractures within a cell*

To determine the combined effect that the patches have on the ability of a cell containing them to conduct flow, the individual patches must be merged together to represent an

Journal Pre-proof

Journal Pre-proof

integrated network of flow passages as shown in Figure 2 (c). This is achieved by analysing the fractures and splitting the branched network into joined sections as a pre-processor step. Only patches that belong to the same joined section are fitted together into larger surfaces. In the example shown in Figure 2 (c), there are two fracture surfaces, each defined by a set of points that lie on the faces of the cell. The average properties of each surface, which represent a portion of the fracture, can be derived from the triangular patches they are constructed from. The average property of each triangle is interpolated from the values at the vertices. When calculating the average of the merged surface, the properties can be averaged using the area of each patch as the weighting. The directionality of each merged surface can also be calculated using the average normal of the triangular patches which is also averaged by area.

The cells that contain fracture surfaces are considered to be part of the pseudo-fracture system (fracture cells) as shown in Figure 2 represented in red, and the properties of these cells need to be modified to account for the presence of the fractures they contain. There are three types of flow that this model must capture: matrix-to-matrix (MM), matrix-to-fracture (MF) and fracture-to-fracture (FF). FUM must represent the fracture-to-fracture and matrix-to-fracture flow by changing the properties of the pseudo-fracture system cells.

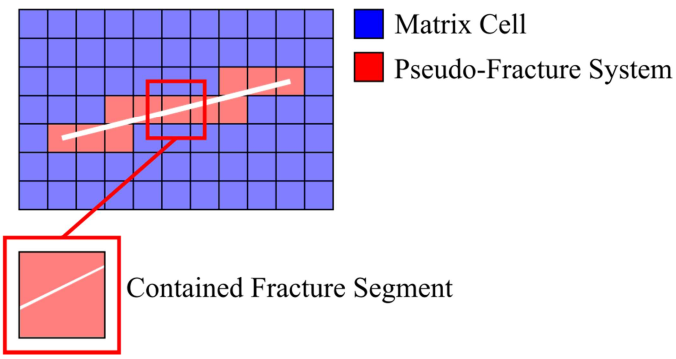


*Figure 2 – A 2D schematic of fracture-grid interaction and the resulting pseudo-fracture system shown in red.*

Figure 3 (a) shows a simple fracture surface, made of triangular patches, located within the framework of a simple finite difference grid. Cells which contain part of the fracture are



Journal Pre-proof

considered part of the pseudo-fracture system and will be altered to reflect the presence of the fracture. This is represented by the solid cells in Figure 3 (b). The pseudo-fracture cells are shown as a wireframe in Figure 3 (c) with the contained fracture surface shown to be contained within these cells.

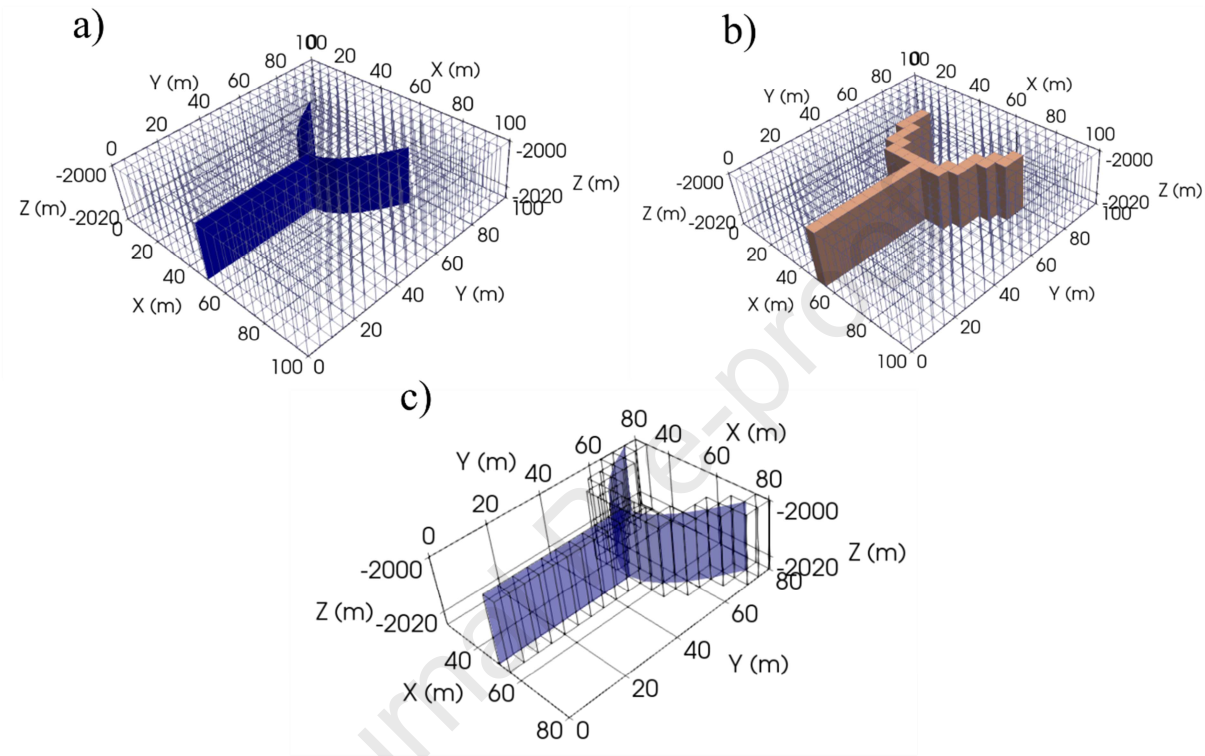


*Figure 3 – Examples of the FUM process: a) shows the fracture plane located inside the grid shown as a wireframe, b) shows the pseudo-fracture system as cells contained within the grid shown as a wireframe & c) Shows the fracture surface within the pseudo-fracture system shown as a wireframe*

The ability of each contained surface within every cell to conduct flow can be determined from the properties of the fracture. In this study we assumed the fracture consists of two semi-infinite parallel plates and the flow is laminar with no complexity of dispersion (Sharifi Haddad et al., 2015) as shown in Figure 4. The one dimensional (e.g., x-direction) single phase volumetric flow rate in the fracture, $q_f$, is given by:

$$q_f = \frac{-w_f^3}{12\mu} h \frac{\partial P_f}{\partial x} \quad (1)$$

Journal Pre-proof

where $w_f$ is the fracture aperture, $\mu$ is the phase viscosity, $h$ is the fracture height and ${\partial P_f}/{\partial x}$ is the pressure gradient applied to the fluid in the fracture.

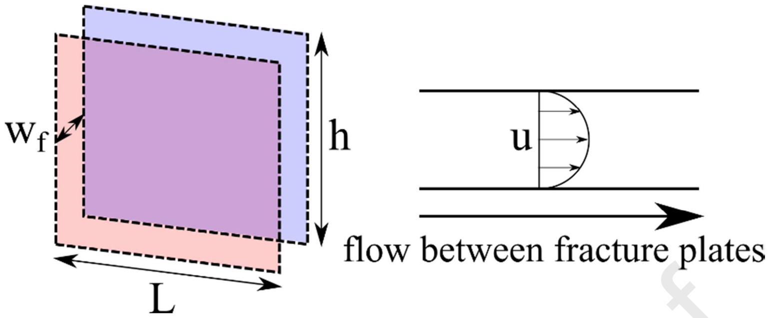


*Figure 4 – Schematic of the parallel plate assumption for flow within a fracture with flow velocity, u, varying across the cross section of the fracture.*

Considering a fractured porous medium using a dual permeability approach the volumetric flow rate is the sum of the matrix and fracture flow.

$$q = q_m + q_f \tag{2}$$

The 1-D volumetric flow rate in the fracture porosity, $q_f$ through a cell is given by,

$$q_f = \frac{-k_f}{\mu} A \frac{\partial P_f}{\partial x} \tag{3}$$

Where $k_f$ is the cell fracture permeability and A is the cross sectional area of the cell being considered. FUM represents the effect of the fracture by calculating the appropriate cell fracture permeability, $k_f$ so that the fracture-fracture transfer is representative of the contained discrete fractures.

Considering a cell containing a single fracture parallel to the direction of flow being considered the following expression can be made by equating Equations (1) and (3):

$$\frac{-k_f}{\mu} A \frac{\partial P_f}{\partial x} = \frac{-w_f^3}{12\mu} h \frac{\partial P_f}{\partial x} \tag{4}$$

This can be rearranged to give the cell fracture permeability as:

$$k_f = \frac{w_f^3}{12}\frac{h}{A} \tag{5}$$

This assumes that the fracture behaves as a channel whereas factors such as the presence of proppants, which partially occupy the volume of the fracture, and fracture surface roughness have a significant impact on flow inside hydraulic fractures. A modified cubic flow equation has been developed to account for fracture roughness (Witherspoon et al., 1980). This approach has been used to calculate fracture permeability in previous fracture propagation studies (Nassir et al., 2014, Zhou et al., 2019). In this study a coefficient of $\alpha = 2 \times 10^{-5}$ will be used to account for the permeability reduction due to proppant as this has a larger effect (Yu et al., 2017). As a result, the permeability is given by:

$$k_f = \alpha \frac{w_f^2}{12}\frac{A_f}{A} \tag{6}$$

where the cross-sectional fracture area, $A_f = w_f h$ refers to the cross section of the fracture on the cell faces in the direction being considered.

To expand this concept to a 3D system, a permeability tensor can be constructed using the average plane normal vector, $\hat{\boldsymbol{n}}_f$, and the unit vectors in Cartesian coordinates $\boldsymbol{e_x}$, $\boldsymbol{e_y}$, $\boldsymbol{e_z}$ as:

$$\boldsymbol{k_f} = \alpha \frac{w_f^2}{12} \begin{pmatrix} |\hat{\boldsymbol{n}}_f \times (\boldsymbol{e_x} \times \hat{\boldsymbol{n}}_f)| \frac{A_{fx}}{A_x} \\ |\hat{\boldsymbol{n}}_f \times (\boldsymbol{e_y} \times \hat{\boldsymbol{n}}_f)| \frac{A_{fy}}{A_y} \\ |\hat{\boldsymbol{n}}_f \times (\boldsymbol{e_z} \times \hat{\boldsymbol{n}}_f)| \frac{A_{fz}}{A_z} \end{pmatrix} \tag{7}$$

Where the area of the intersection between the fracture and the plane of the cell faces are given by $A_{fx}$, $A_{fy}$, and $A_{fz}$. When a fracture passes through two neighbouring sides of a cell then the permeability needs to be enhanced in at least two directions. If this occurs and the fracture is nearly perpendicular to one of the grid axes, the result would be a permeability tensor with one component very close to zero which would result in the pseudo-fracture

Journal Pre-proof

system being poorly connected. To resolve this, when the fracture crosses two neighbouring cell faces the apparent permeability is assumed to be the same in all directions normal to the cell faces that the fracture crosses. The magnitude of the apparent permeability is considered to be the largest of the components. This is only applied when a fracture passes through two neighbouring cell faces.

Equation (7) gives the apparent permeability of a cell containing a single fracture. However, one cell may contain several fractures. Similar to previous studies, the effects of multiple fractures contained by a cell can be summed (Nassir et al., 2014, Sakhaee-Pour & Wheeler, 2016):

$$\boldsymbol{k_f} = \sum_{i=1}^{n} \boldsymbol{k_f}_i \qquad (8)$$

The matrix-to-fracture mass transfer for phase j, $t_{jmf}$, is calculated using the equation:

$$t_{jmf} = \sigma V \frac{k_{rj}\rho_j}{\mu_j}(P_{jm} - P_{jf}) \qquad (9)$$

Where V is the grid block volume, $\sigma$ is the shape factor, $k_{rj}$ is the relative permeability of phase j, $\rho_j$ is the phase density, $\mu_j$ is the phase viscosity, $P_{jm}$ is the phase pressure in the matrix and $P_{jf}$ is the phase pressure in the fracture. Dual-permeability simulators consider the cell to contain sets of fractures that are parallel to the grid axes to calculate matrix-fracture mass transfer. The shape factor is calculated using the Gilman-Kazemi formula:

$$\sigma = \left(\frac{k_{mx}}{l_x^2} + \frac{k_{my}}{l_y^2} + \frac{k_{mz}}{l_z^2}\right) \qquad (10)$$

Where $k_{mx}, k_{my}, k_{mz}$ are the matrix permeabilities and $l_x, l_y, l_z$ are the fracture spacings, in the x-, y- and z-direction. Therefore, to calculate the matrix-to-fracture mass transfer the fracture spacing is also required. At this point, the complex fractures have been upscaled and are represented by permeability enhancements in the x-, y- and z-direction that capture the conductivity of the complex fracture network contained within each cell as calculated by Equation (8). FUM also evaluates the fractures contained by each cell to determine if this is most similar to a single fracture plane with a normal in just one direction such as the x-direction as shown in Figure 6 (a) where $l_x = \Delta x$, if the fracture is normal to the y- or z-direction then $l_y = \Delta y$ and $l_z = \Delta z$, respectively. If the cell contains fractures that have significantly different normal vectors and orientations then FUM determines if this is best represented by two orthogonal fracture planes, Figure 6 (b) or by three orthogonal fracture planes, Figure 6 (c). In this study only vertical fractures are considered. From the discrete fracture input data, FUM also calculates how many fractures cross the cell in each direction, e.g. normal fractures to the x-direction $Nf_x$, and when there are multiple planes in the same direction the spacing is divided by this number so that $l_x = {}^{\Delta x}/_{Nf_x}$.

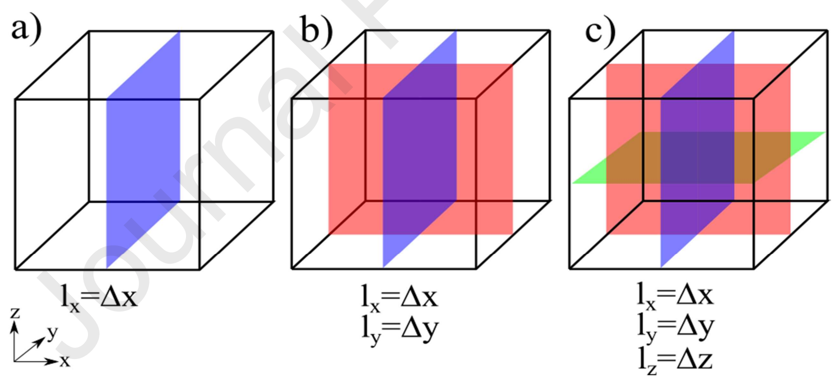


*Figure 5 – Fracture spacing assumption in FUM for calculating shape factor for matrix-fracture transfer with fracture(s) normal to the a) x-direction, b) x- and y-direction, or c) x-, y- and z- direction*

## 3. Results and Discussion

The method developed in this study (FUM), represents an opportunity to model production from complex hydraulic fracture networks in finite difference-based multiphase flow simulators. Firstly, the upscaling process can be demonstrated using simple fracture segments and simple sensitivity tests to show the behaviour of the system with different grid sizes and fracture properties. In the next part of this study, we tested the performance of FUM against

Journal Pre-proof

Journal Pre-proof

field data, and the details are presented. The effect of natural fractures and the resulting complex fracture networks are also studied. Finally, a test case is presented to demonstrate the full complexity that FUM can incorporate and highlight the novelty of this method.

In this study, it is assumed that natural fractures are planes of weakness that are cemented. They only affect the geomechanical properties of the system and do not contribute to the hydrodynamic properties of the formation unless reactivated by the hydraulic fractures.

The relative permeabilities of the fracture and the matrix are shown in Figure 6 (Daigle et al, 2015). Water saturation in the matrix cells containing the fracture network are increased to represent the water leak-off volume during the hydraulic fracturing resulting in a reduced gas relative permeability around the fractures. The initial water saturation of the fracture is assumed to be 1.

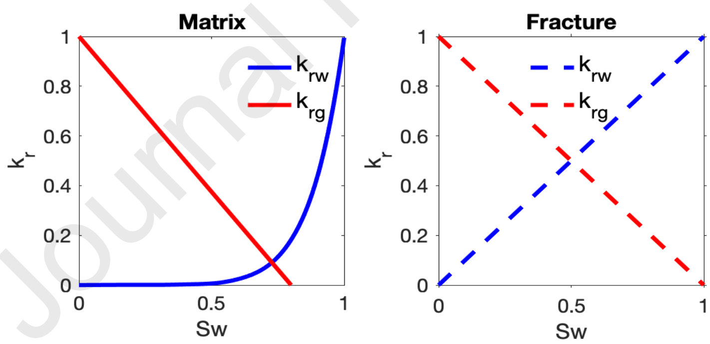


*Figure 6 – Relative permeability curves for the matrix and fracture (Daigle et al., 2015)*

There are other phenomena that must be considered when modelling gas production from shale reservoir. The matrix and fracture permeabilities are pressure dependant and calculated using the equations below,

$$\boldsymbol{k_m} = \boldsymbol{k_{mi}} e^{-\gamma_m (P_{mi} - P_m)} \quad (11)$$

$$\boldsymbol{k_f} = \boldsymbol{k_{fi}} e^{-\gamma_f (P_{fi} - P_f)} \quad (12)$$

Journal Pre-proof

Where $\boldsymbol{k_{mi}}$ and $\boldsymbol{k_{fi}}$ are the initial matrix and fracture permeabilities before production begins, $P_{mi}$ and $P_{fi}$ are the initial matrix and fracture pressures before production begins. $\gamma_m$ and $\gamma_f$ are the matrix and fracture permeability modulus, respectively. The values used in this study for these parameters are provided in Table 1 (Zhang & Emami Meybodi, 2020).

An extended Langmuir adsorption isotherm is used to take into consideration the desorption of hydrocarbons from the organic material of the shale (Arri et al., 1992, Hall et al., 1994). The number of moles of component i adsorbed per kg of rock is calculated as,

$$w_i = \frac{w_{i,max} B_i P}{1 + B_i P} \tag{13}$$

Where $w_{i,max}$ is the maximum number of adsorbed moles of component i per kg of rock, $B_i$ is the Langmuir isotherm parameter. This is fit against field data from Yu et al. 2017 using the values of $w_{i,max}$ and $B_i$ in Table 1. Although it has been shown that BET isotherms can capture this process more accurately, this was not available in the reservoir simulator used here. A Klinknberg correction, $P_{kr}$ is made for slip flow at low pressures and detailed in Table 1 (Letham & Bustin, 2015) For flow in the fractures the non-Darcy effect is considered using the Forchheimer correction to Darcy's law (Forchheimer, 1901). The beta correction is calculated as below,

$$\beta = \frac{\alpha_g}{(kk_{rg})^{N1p}} \tag{14}$$

The parameters $\alpha_g$ and $N1_g$ are detailed in Table 1 and $k_{rg}$ is the gas relative permeability (Evans & Civan, 1994).

Journal Pre-proof

Table 1 – Production simulation reservoir parameters

| Property | Value |
|---|---|
| $\gamma_m\ (kPa^{-1})$ | $4.35 \times 10^{-6}$ |
| $\gamma_f\ (kPa^{-1})$ | $4.35 \times 10^{-5}$ |
| $w_{CH4,max}\ (mol/kg)$ | 0.23 |
| $B_{CH4}\ (kPa^{-1})$ | $2.9 \times 10^{-4}$ |
| $P_{kr}\ (kPa)$ | 500 |
| $\alpha_g\ (m^{-1})$ | $4.76 \times 10^{9}$ |
| $N1_g$ (-) | 1.021 |
| Initial water saturation of fracture (-) | 1.0 |
| Shale density $(kg.m^{-3})$ | 1992 |
| Fracture porosity (-) | 0.001 |

**3.1 Simple Fracture Segments**

Simple test cases can be constructed with a geometry of 100×100×25 m and shown in Figure 7. The well is considered to be located horizontally along x-direction (at y = 0) and the hydraulic fracture originates from the points x = 50 m, y = 0 m. The hydraulic fracture is vertical and fully intersects the grid in the vertical direction, i.e. the fracture has the same height as the cell thickness. For these simple cases a single layer thick reservoir is considered (i.e., 2D systems). The fractures have a constant aperture of 1 mm.

Figure 7 shows the resulting cell permeabilities in the x- and y-direction of the simple test fracture segments with a 4×4×25 m cell size. The planar fracture in test case 1 has the simplest geometry in which the fracture cells only contain an altered permeability component in the y-direction. Test case 2 contains fracture segments in different directions but these are still perpendicular to the grid axes. Whereas, the fracture segments of test cases 3 and 4 result in some cells having a component in the x- and y-direction.

Journal Pre-proof

Journal Pre-proof

The FUM process can generate different pseudo-fracture networks if the spatial location of the grid changes with respect to the fractures. This can also result in symmetrical fractures being upscaled to unsymmetrical pseudo-fractures.

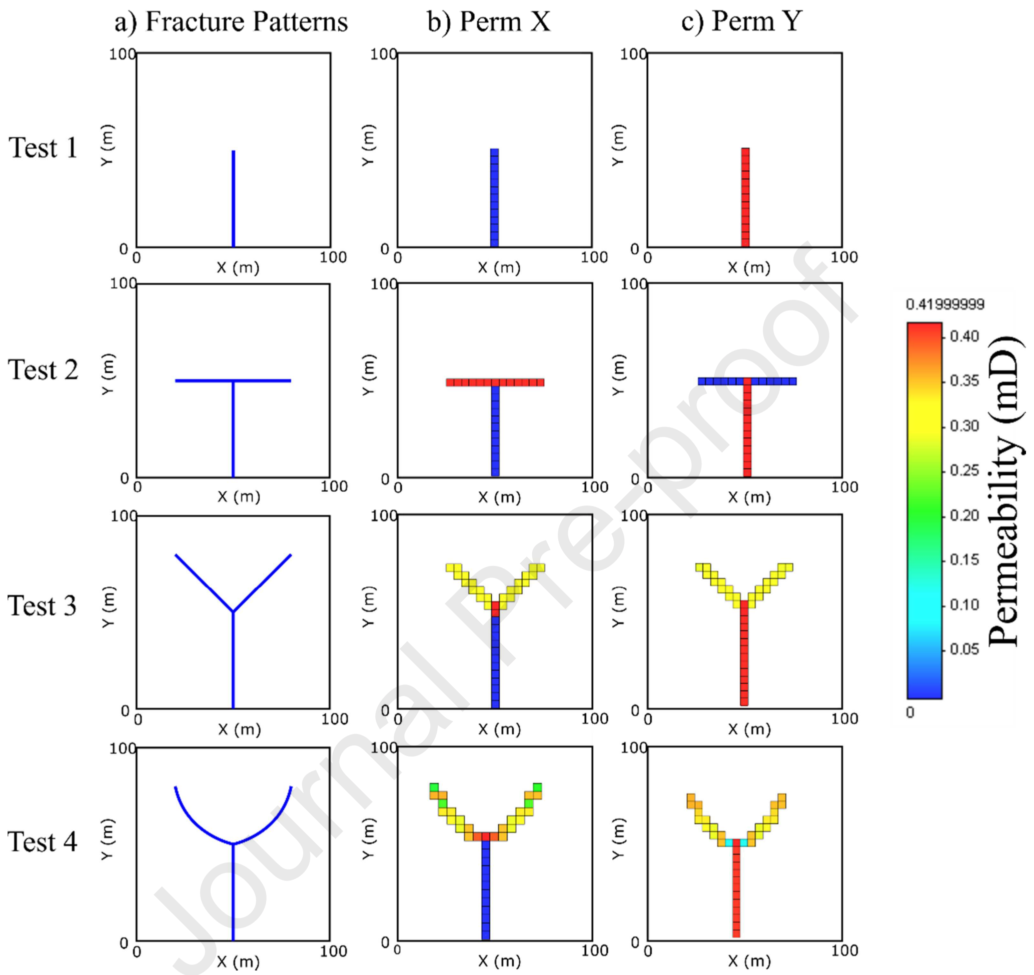


*Figure 7 – Application of FUM in several simple fracture segments (Tests 1-4): column a is an output fracture pattern from FEM simulators with constant aperture of 1mm (input to FUM), columns b and c are representing permeabilities in x- and y-direction for the fractures in finite difference-based simulators (output of FUM)*

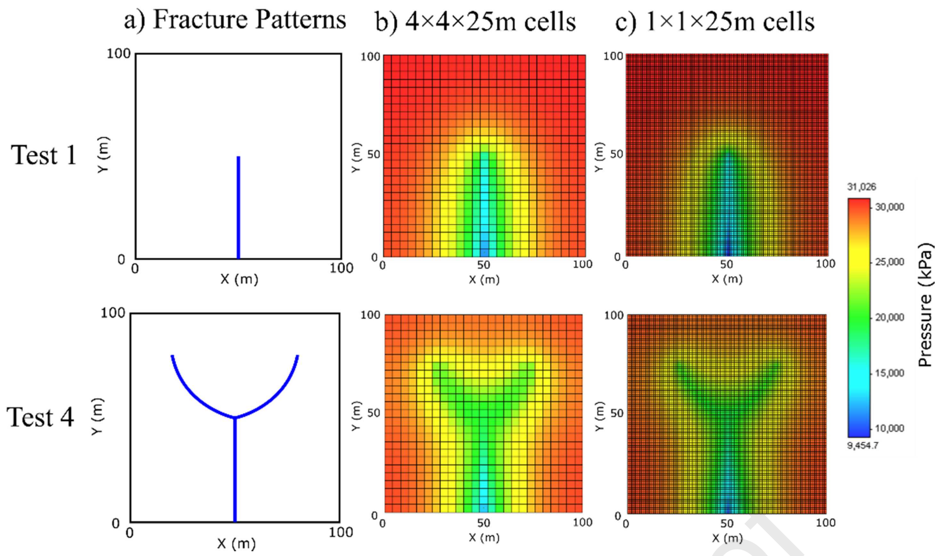


*Figure 8 – Pressure distribution in matrix blocks after 10 months of production for two different test cases: column a is fracture pattern output from FEM simulators with constant aperture of 1mm, and columns b and c are pressure distributions in models with different grid sizes*

The upscaled finite-difference grids produced by FUM were exported to CMG-GEM to model gas production using a matrix permeability of 0.001 mD, a porosity of 0.12 and other simulation parameters as Table 1. A bottom hole pressure (BHP) schedule decreasing from 29,150 kPa to 3,447 kPa is used. The pressure profiles of test cases 1 and 4 after 10 months of production is shown in Figure 8 for two cell sizes. This shows the ability of FUM to represent the fractures with some complexity even with coarse grids. Figure 9 also shows cumulative production obtained using different grids. In these test cases, the effect of coarsening the grid has limited impact on cumulative production. When more complex fracture networks and multiple fractures are considered, the coarseness is expected to present more challenges due to the oversimplification of fracture geometry.

Journal Pre-proof

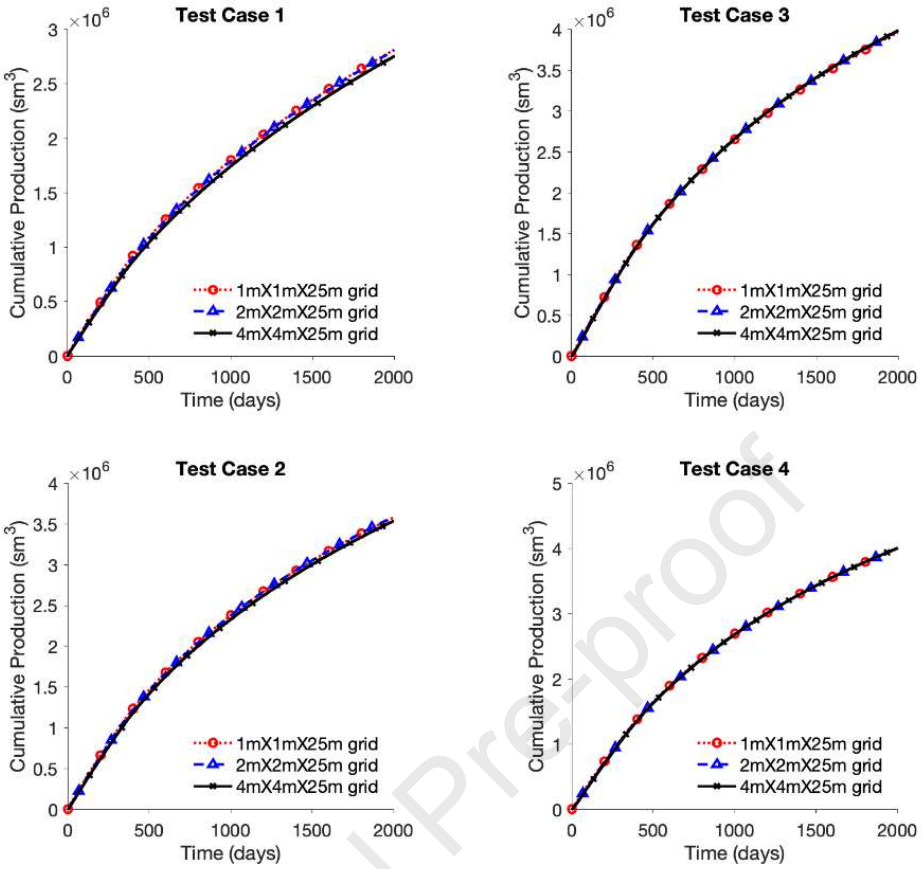


*Figure 9 – Cumulative production from simple fracture test cases with different cell sizes*

The effect of fracture aperture on cumulative production is also shown in Figure 10. In this case same properties as the previous case (except fracture aperture) were used in a model with 1×1×25 m cells. Fracture aperture controls the ability of the fracture to conduct flow and therefore a larger fracture aperture results in higher recovery. The pressure distribution in matrix blocks during production with different fracture apertures is shown in Figure 11. This shows that when the fracture aperture is large the pressure difference along the matrix parallel to the length of the fracture is nearly zero. As the fracture aperture becomes smaller the pressure difference gets larger until there is no pressure change along the length of the fracture as it has no effect on the ability to transmit flow.

Journal Pre-proof

Journal Pre-proof

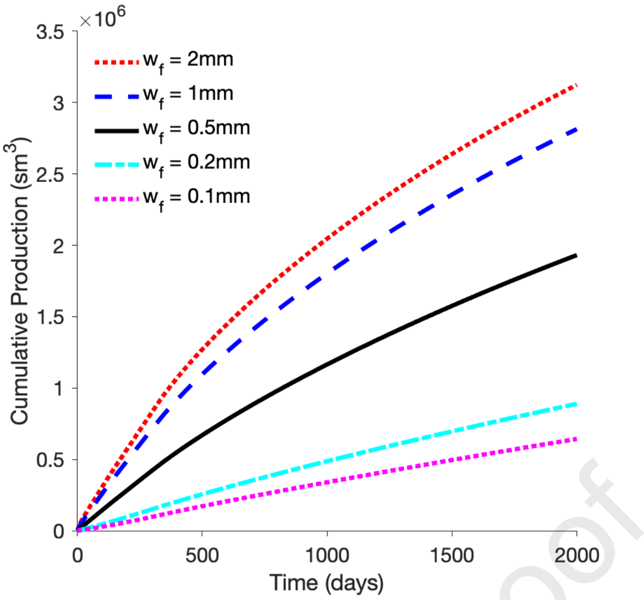


*Figure 10 – Cumulative production for test case 1 with different fracture apertures.*

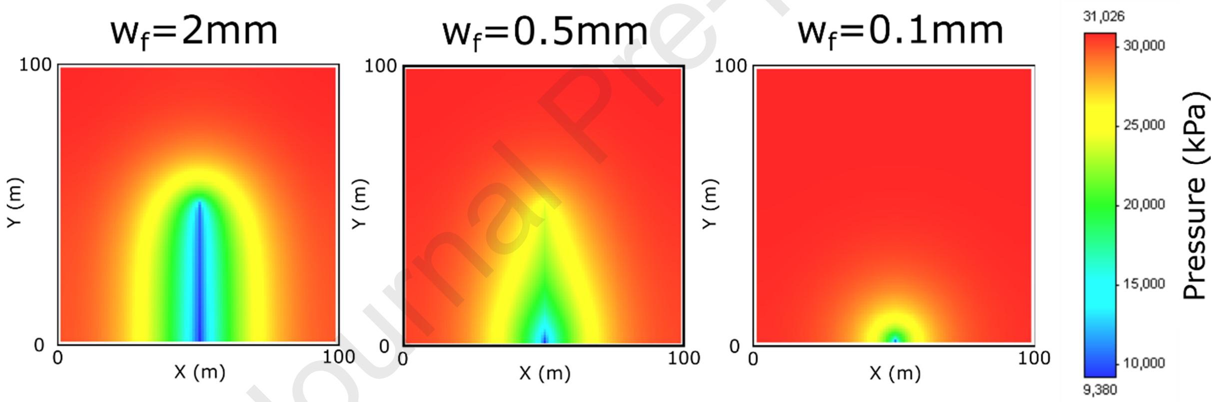


*Figure 11 – Pressure distribution in matrix blocks after 300 days with different fracture apertures. Cell size 1×1×25m.*

### 3.2 FUM Comparison with the Field Data

The FUM is tested against field data to compare the accuracy of the model prediction. The field description, fracture stimulation and production parameters from a single shale gas well have been detailed in a previous study (Yu et al., 2017). An unconventional fracture model (Petrel Kinetix, Schlumberger 2019) is used to generate a discrete fracture network using the parameters as detailed in Table 2. The output of the unconventional fracture model (FEM) is used in our model (FUM) to generate an upscaled finite-difference based computational grid which is exported to the reservoir simulator, in this study CMG-GEM, to model gas production. The grid could be exported to any conventional multiphase flow reservoir simulator, and this approach could be used with the output of any discrete fracture propagation model.

The horizontal well is approximately 850 m in length and completed with 11 fracturing stages. Each stage is spaced 47 m apart and completed with 4 perforation clusters, of 16 perforations each, spaced 16 m apart. The total volume of injected slickwater is 14,308 $m^3$ at a rate of 9.5 $m^3$/min, along with 2.18 million kg of sand proppant.

*Table 1 – Reservoir properties*

| Property | Value |
|---|---|
| Permeability ($mD$) | 0.0008 |
| Porosity (-) | 0.12 |
| Maximum Horizontal Stress ($kPa$) | 51,200 |
| Minimum Horizontal Stress ($kPa$) | 48,263 |
| Initial Reservoir Pressure ($kPa$) | 31,026 |
| Initial Water Saturation (-) | 0.10 |
| Poisson Ratio (-) | 0.23 |
| Young's Modulus ($kPa$) | $2.06 \times 10^7$ |
| Reservoir Temperature (℃) | 55 |
| Shale Gas Composition | $CH_4$ |

Journal Pre-proof

There is some information required for the unconventional fracture model that was not available for this field case, therefore typical field values for them are assumed. The production tubing is assumed to have an inside diameter of 146 mm. It is assumed that the formation is normally pressurized, therefore, the depth can be interpreted from the reservoir pressure as 3,160 m. Assuming an overburden density of 2,700 kg/$m^3$, the overburden stress is approximately 67,000 kPa. The unconventional fracture model requires a detailed pump schedule including the slickwater properties, proppant size and proppant concentration. Typically, proppants are initially injected at low concentrations and ramped up, and a range of different proppant sizes are also usually used. As this data has not been supplied a generic pump schedule is used with a constant injection rate. Following a pad stage with no proppant, 80/100 mesh sand is injected ramping up from 30 to 300 kg/m$^3$, and then 40/70 mesh sand ramped up from 60 to 350 kg/m$^3$. The total volumes of sand and slickwater match those reported from the case study.

The previous study used the thickness of the reservoir as a fitting parameter and reported this to be 85 feet (25 m). Therefore, in this study, the fracture maximum height and reservoir thickness are assumed to be 25 m. An intrinsic leak-off coefficient is used to match the fracture geometry with the previous study as flow back volumes are also not reported. A good match is found with a value of 6, but this is not unique and requires calculating before executing any project.

The gas production rate is shown in Figure 12, which shows a reasonable match with field data from the first 120 days of production. A model with 1,150×600×1 active grid cells each with a dimension of 1×1×25 m. The production rate predicted by the model shows a peak for the first 10-15 days. However, the reasonable match after 20 days should give confidence in the model and the overestimation over the first few days will have little effect over years of production modelling. This overestimation (early peak) might be due to a more complex water distribution in the matrix blocks around the fractures following stimulation. This results in a reduction of relative permeability around the hydraulic fractures reducing the ability of gas to flow into the fractures and causing the lower production rate observed in comparison to the simulation. Other physical effects such as rock and fluid compressibility, and changes in fracture aperture during early production may also contribute towards the difference between the field data and predicted by FUM. To validate these results, further field data or microseismic data is required.

Journal Pre-proof

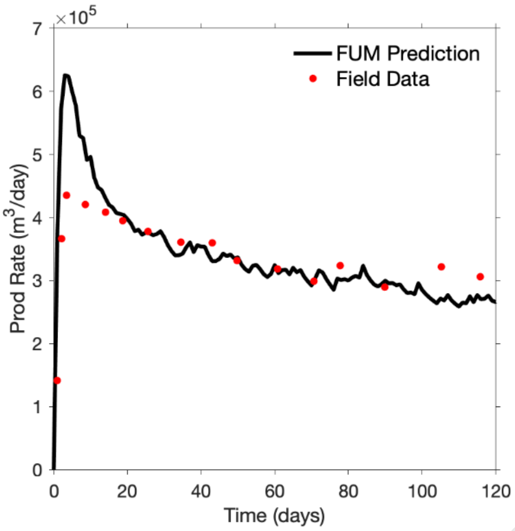


*Figure 12 – A comparison of simulated production rates with the field data*

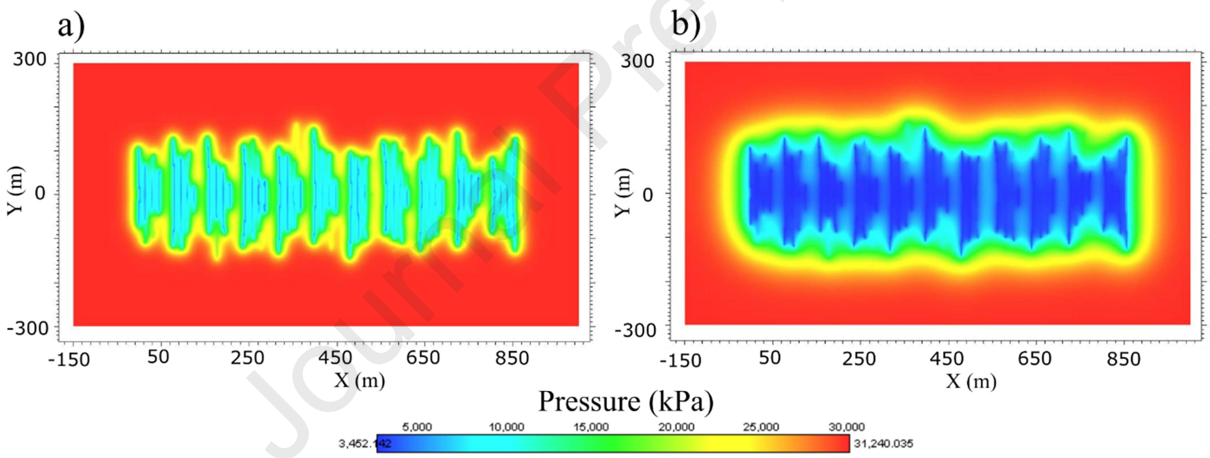


*Figure 13 – Pressure profiles of the reservoir (matrix blocks) after a) 300 days and b) 2,000 days. Cell size 1×1×25m.*

The pressure profile in the formation during recovery is shown in Figure 13. Although the fracture geometry is simple, it is more complex than the previous study which only considered the stress shadow effect in each stage and ignored the interaction between different stages. The hydraulic fracture geometry is summarised and compared with Yu et al., 2017 in Figure 14. This shows the fracture lengths are similar, but there are differences. In addition to this, all subsequent stages are heavily impacted by the stress shadow of the previous stage. As a result, in all subsequent fracture stages the fracture closest to the previous stage is prevented from propagating very deeply into the reservoir and fractures further away tend to propagate more deeply. On the other hand, Yu et al. only calculated the fracture geometry for the first stage and then repeated this for all subsequent fracture stages. Therefore, the input fracture models in all of our simulations are produced by Kinetix. In this work, we do not study the propagation of the fractures as the main focus here is the incorporation of fracture networks in finite difference simulators to determine the impact on gas recovery.

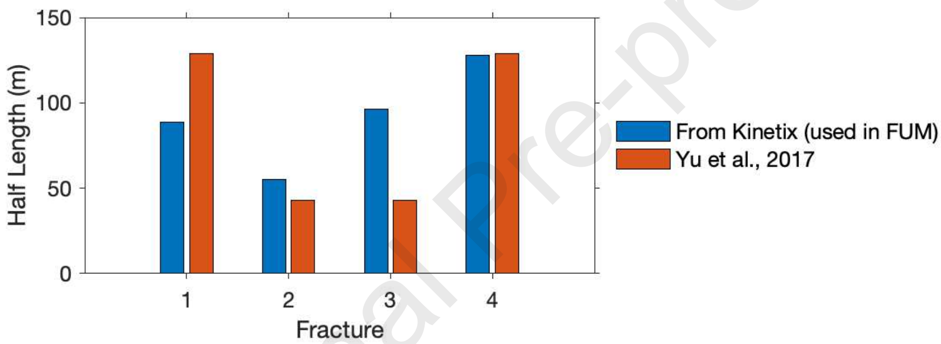


*Figure 14 – Half lengths of fractures in the first stage of this study compared with Yu et al., 2017*

Journal Pre-proof

Once the fracture patterns are produced by Kinetix for a hydraulic fracturing operation, and they are inputted to the FUM, then this upscaling simulator calculates the fracture conductivity at each spatial point along the fracture from the aperture at that point. As a result, the pressure depletion changes along the fractures. In this study, fracture conductivity in the vertical direction is averaged because the fracture planes are upscaled into a single layer thickness grid. However, this can be incorporated in the FUM for 3D models, as this could have a big impact because proppants settle due to gravity and fracture aperture tends to be greatest at the bottom of the fracture. This can be considered as an advantage of current modelling procedure over existing models which will be explored in the future.

Journal Pre-proof

Figure 15 shows the cumulative production of the field case using different grid sizes. The effect of cell size on cumulative production is very limited for cell sizes up to 8×8×25 m. The difference in the upscaled permeabilities is also shown in Figure 16 for grids with 4×4×25 m cells compared to 1×1×25 m cells. Coarse grids are likely to reduce accuracy because they begin to oversimplify the complex fracture geometry, especially when this method is used for more complex fracture networks. Therefore, larger cell sizes were not tested and for the remainder of this study a cell size of 2×2×25 m is used.

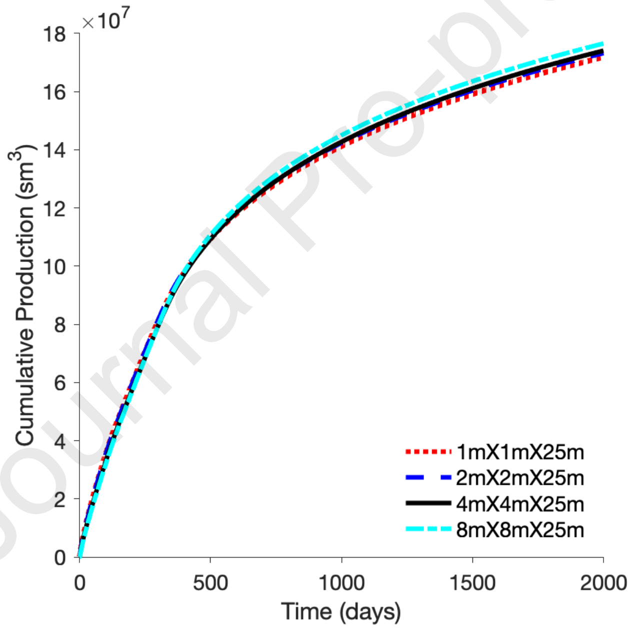


*Figure 15 – Cumulative production with different cell sizes*

Journal Pre-proof

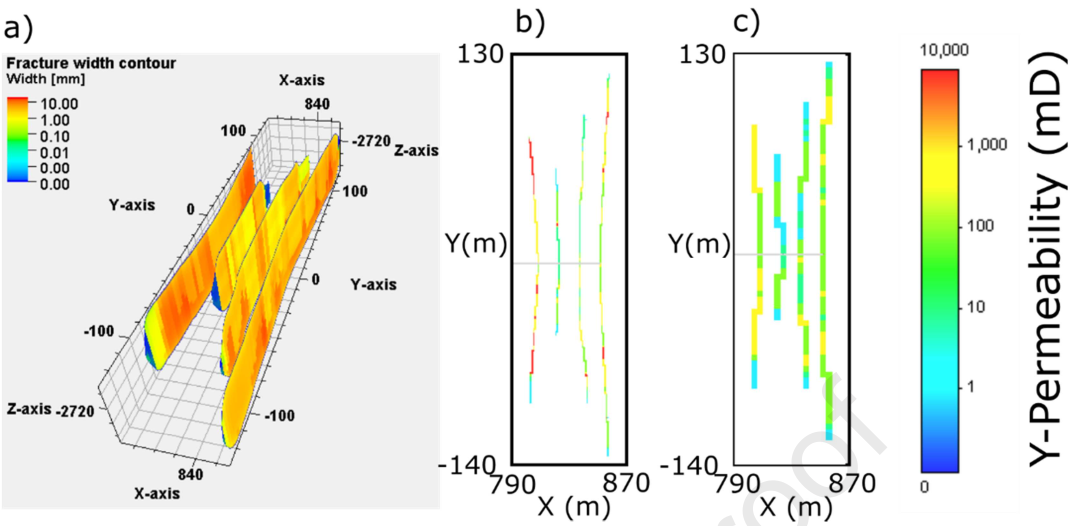


*Figure 16 – Stage 1 of the field case a) exported fracture aperture, and upscaled fracture permeabilities in the y-direction for b) 1×1×25 m cells &c) 4×4×25 m cells*

### 3.3 Complex Fracture Networks

Natural fractures and other planes of weakness in the reservoir have been shown to significantly affect the propagation of hydraulic fractures often resulting in highly complex fracture networks (Wu & Olson, 2015, Dahi-Taleghani & Olson, 2013, Dahi-Taleghani & Olson, 2011). The resulting complex fracture networks may affect the hydrocarbon production from such reservoirs. One of the applications of this study is to use the developed method, FUM, to quantify the effect natural fractures have on propagation of hydraulic fractures and consequently on gas production. These results can be used to estimate the uncertainty if the existing natural fracture networks are poorly defined before hydraulic fracturing takes place and could also help determine the possible success of a project, through optimising well placements and fracking stages.

Synthetic natural fracture networks are introduced to the scenario in which the FUM was tested against field data. A single set of fractures is defined by the fracture length (L), fracture spacing (S), and fracture angle (θ), measured from the direction of maximum horizontal stress

Journal Pre-proof

which is perpendicular to the well trajectory, as shown in the Figure 17. The natural fractures are only specified with a 2D geometry and assumed to have a height that fully penetrates the formations being hydraulically fractured. The fractures are distributed by assigning the mean and standard deviation of the length, spacing and angle.

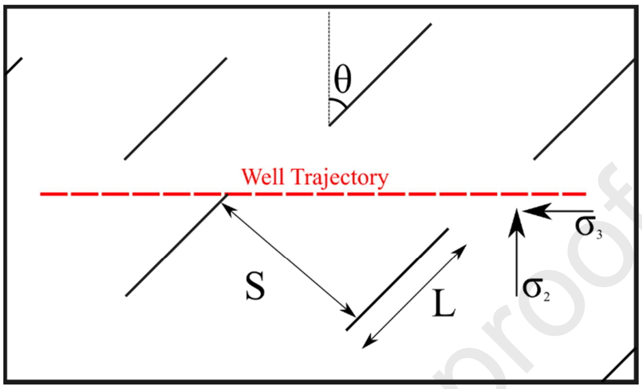


*Figure 17 – Schematic of a single natural fracture set distribution relative to the well trajectory*

As discussed earlier, the hydraulic fractures will open in the configuration which requires the least amount of energy. During hydraulic fracturing this means that fractures open perpendicular to the least principal stress. The fracture strength of a material is the ability of a rock to resist failure. However, the fracture strength of a natural fracture is less than the virgin formation and therefore it may require less pressure to propagate a hydraulic fracture along a pre-existing plane of weakness, such as a natural fracture, even though a component of the maximum horizontal stress is opposing it. In this study, the fracture strength of natural fractures is assumed to be approximately 75% that of the shale to represent partially cemented fractures.

In a previous study by Yu, Hu et al. (Yu et al., 2017) for which the reservoir properties were used for this study, the reported maximum and minimum horizontal stresses are very similar. Therefore, hydraulic fractures are likely to propagate easily along the natural fracture networks introduced in this study. To understand the effect of natural fractures, complex behaviour of natural fractures and differential stress needs to be combined to find the fracture propagation mode. If there is a larger differential stress, it is more likely that the fracture will propagate perpendicular to the least principal stress and the natural fractures will have less impact.

Synthetic fracture network realisations are not unique. Therefore, multiple simulations are run using different realisations of each fracture distribution and averaged to increase the reliability of results. These sensitivity analyses and the corresponding fracture networks are not validated against any field data as the aim is to understand the effect of each parameter on production forecasts.

The reservoir properties used in simulations are detailed in Tables 1 & 2 with 172,500 cells each with a size of 2×2×25m in x-, y- and z-direction (575×300×1). All CMG-GEM simulations were performed on a desktop computer with an i5 quad-core processor (3.2 GHz) and 8 GB of RAM. Each simulation required approximately 1-4 hours to run 2000 days of production. Highly complex fracture networks require higher CPU time and smaller time steps to reach convergence. The FUM code only runs on a single core and the upscaling time depends on the polygon count of the fracture network which increases with size and complexity. In our study, the fracture upscaling was performed using the same machine detailed above, in under one hour.

### 3.3.1 Natural Fracture Orientation

Natural fractures in the formation could have been formed at any time during the millions of years since the sediment was deposited. During the geological history of the formation the tectonic stress state could have been very different to the present-day, meaning fractures could be present in almost any orientation. The orientation of natural fractures may affect the propagation of hydraulic fractures. A 2D areal profile of the hydraulic fracture network generated using synthetic natural fracture networks with θ = 0° and θ = 90° is shown in Figure 18, which clearly shows the increase in complexity by changing the orientation of natural fractures. With a small angle between natural fractures and maximum horizontal stress, hydraulic fractures propagate deeper into the formation than when the natural fractures are perpendicular to the maximum principal stress. For each case three natural fracture realisations were generated and run through the full FUM workflow, generating three different production profiles which can be averaged. The unconventional fracture model also captures proppant transport, and the proppant distribution is also different in these cases, but this is not investigated further in this study.

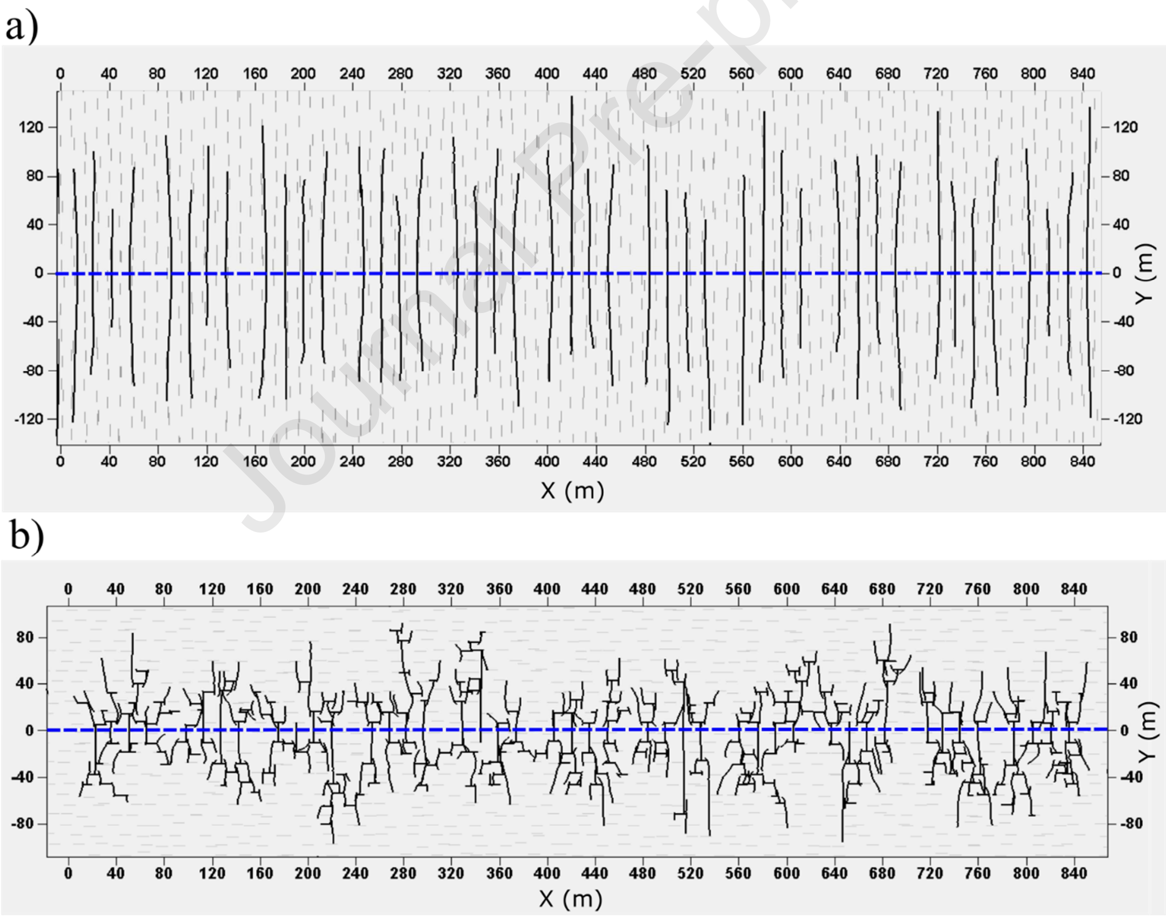


*Figure 18 – Areal view of hydraulic fracture networks when a) θ=0° and b) θ=90° for L=10m, S=10m and FS=800 (The well trajectory is shown as the blue dotted line)*

These fracture networks are upscaled by using the FUM, to model gas production and the effect of natural fracture orientation on cumulative production, as shown in Figure 19. The

Journal Pre-proof

natural factures have an average length of 10 m and an average spacing of 10 m. However, a small deviation is applied to the distribution to increase the complexity. This clearly shows that cumulative gas production is higher when the fracture angle is smaller. Cumulative production is shown to have been changed by up to 19% just because of fracture orientation. The presence of natural fractures with a larger angle with the maximum horizontal stress orientation leads to hydraulic fractures that do not penetrate deeply into the formation. As a result, gas is only produced from a smaller stimulated region around the well, and cumulative recovery is reduced.

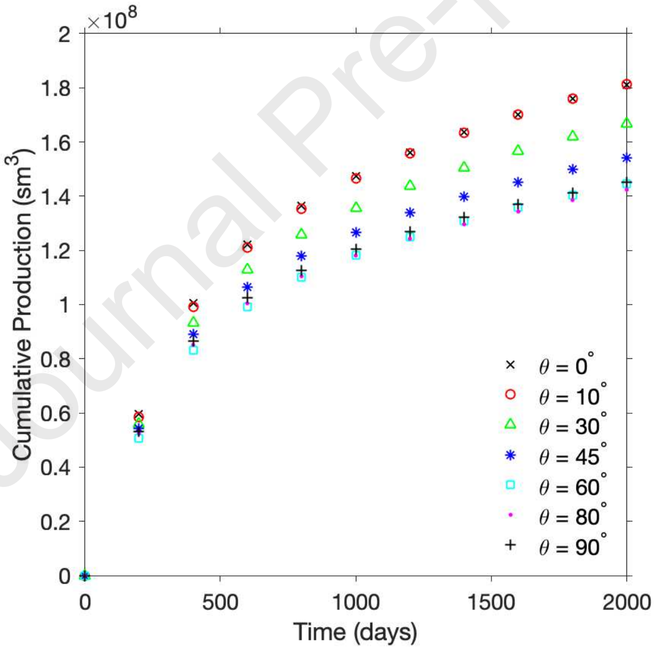


*Figure 19 – Cumulative production with natural fracture networks with different orientations relative to the well trajectory with L=10m, S=10m.*

The pressure profile in the formation after 300 days is shown in Figure 20 where the natural fractures are at an angle of 0° or 90° with the direction of maximum horizontal stress. This clearly demonstrates that the simple and deep-penetrating fractures are able to recover gas from larger stimulated volume in the formation, resulting in higher recovery. There are some fractures that are well-connected to the well, resulting in the bigger pressure drops as shown

Journal Pre-proof

by the dark blue regions. However, some parts of the system are less well-connected due to the small fracture aperture. As a result, the pressure is still reduced but not as much as in other regions, shown by the green regions.

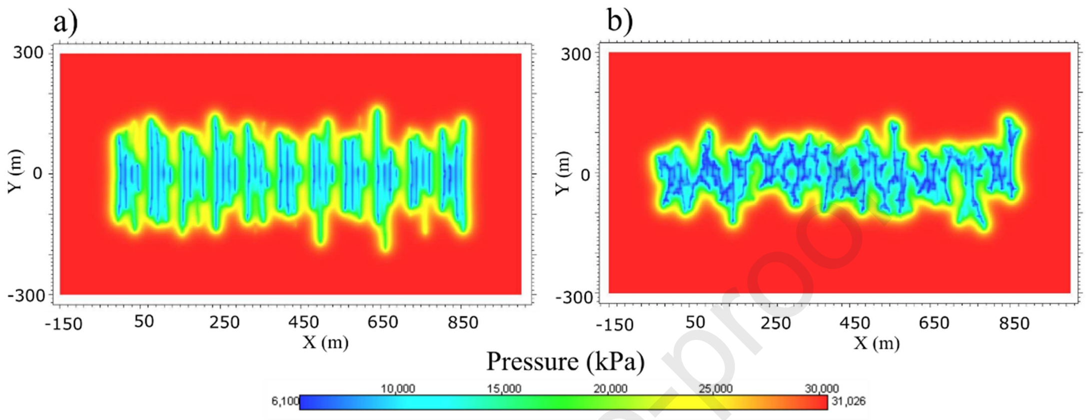


*Figure 20 – Pressure profiles of the reservoir (matrix blocks) after 300 days of production when a) θ=0° and b) θ=90° and S=10m, L=10m. Cell size 2×2×25m.*

The cumulative production can also be expressed as a percentage reduction from the case with no natural fractures, as shown in Figure 21. Each curve represents the average production from multiple realisations at a different time. Cumulative gas production is minimum with an orientation of 80°, and it is reduced by almost 17% compared to base case with no natural fractures, while cumulative gas production is maximum for the case with natural fractures at 0°-10°, which shows a 2% increase in recovery compared to the base case after 2,000 days. At angles between 50° and 90° the production reduces by 12-17%. Cumulative production is not the lowest at 90° which can be explained by the fact that the hydraulic fractures are more likely to cross the natural fractures rather than propagating along them, resulting in simpler fracture geometries that penetrate slightly deeper into the formation.

Based on these results, it is suggested that an optimal gas production is achieved when the angle between natural fractures and the maximum horizontal stress is smaller, whilst large

Journal Pre-proof

angles result in a poorer recovery. The greatest change in gas production occurs at natural fracture angles between 20° and 60°, and it is suggested that if the natural fractures occur within this range the natural fracture distributions should be set up more carefully to minimise the uncertainty.

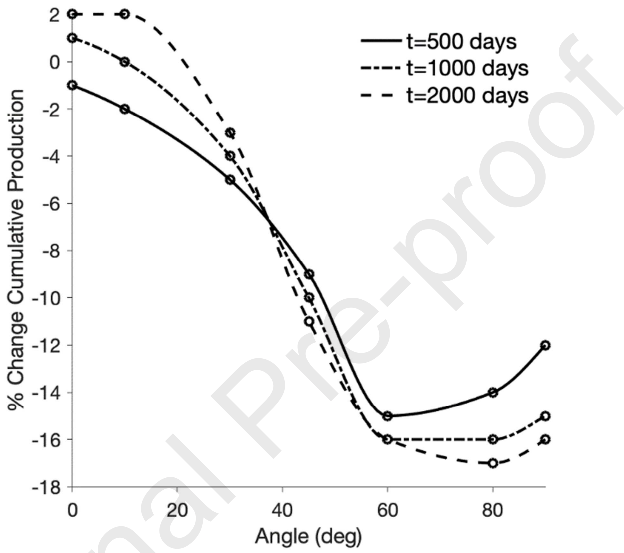


*Figure 21- Percentage change in cumulative production when S=10m and L=10m in comparison with the case without natural fractures*

Journal Pre-proof

It should be noted that in these test cases the maximum and minimum horizontal stresses are very similar. When there is a larger differential stress the impact of the orientation of natural fractures will most likely be different.

### 3.3.2 Natural Fracture Length

Complexity of the fracture network increases when the hydraulic fracture meets a natural fracture and propagates along it. A longer natural fracture results in a larger deviation from the path the hydraulic fracture would have taken. Therefore, shorter fractures result in simpler geometry. Cumulative gas production with different fracture lengths is shown in Figure 22.

Journal Pre-proof

This shows that a shorter fracture length results in a slightly increased recovery but once the length is greater than 10 m there seems to be very little impact on recovery, and therefore fracture length is unlikely to cause much uncertainty in predicting production.

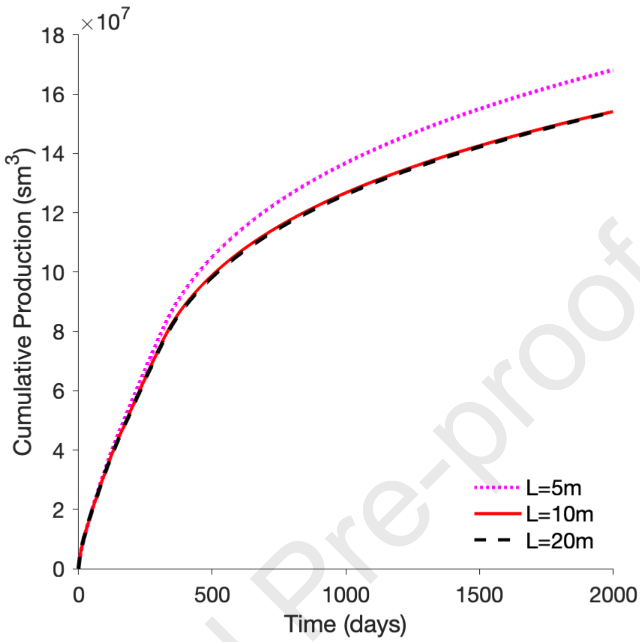


*Figure 22 – Cumulative production with varying natural fracture length when θ=45°, S=10m*

### 3.3.3 Natural Fracture Spacing

Natural fracture spacing affects the density of fractures and if there is high density of natural fractures, there will be a higher chance of interaction between them and propagating hydraulic fractures, which leads to even more complex hydraulic fracture networks. The effect of natural fracture spacing on gas production from the hydraulically fractured well is shown in Figure 23. This clearly shows a trend of decreasing cumulative gas production with decreasing fracture spacing. As seen previously, by increasing the interaction of natural fractures and hydraulic fractures, the hydraulic fractures penetrate less into the formation, which can explain the reduction in gas production shown in Figure 23. This is supported by the pressure profiles in Figure 24 which compares the regions that have been accessed by

Journal Pre-proof

hydraulic fractures when S=5m (high natural fracture density) and S=20m (low natural fracture density).

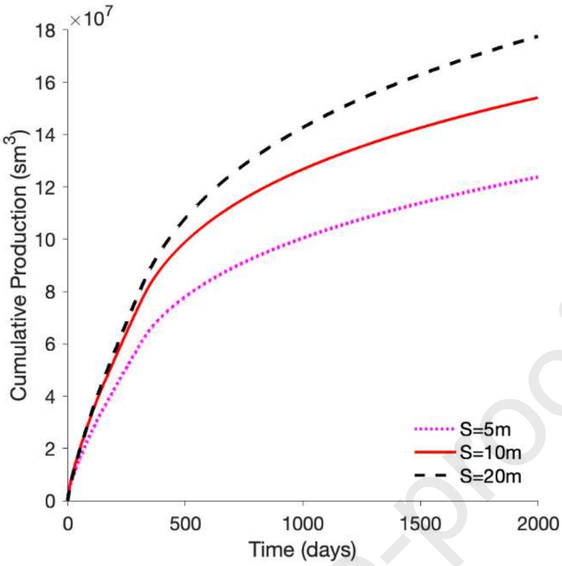


*Figure 23 – Cumulative production with varying fracture spacing when θ=45°, L=10m, FS=800*

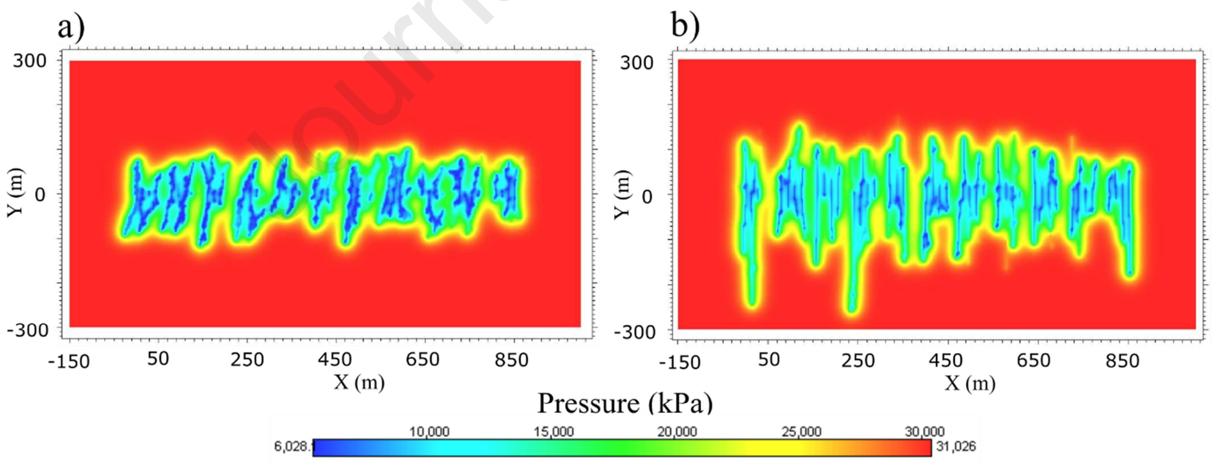


*Figure 24 - Pressure profiles of the reservoir (matrix blocks) after 300 days of production when a) S=5m and b) S=20m and θ=45° and L=10m. Cell size 2×2×25m.*

The cumulative gas production is also expressed as a percentage reduction compared to the case with no natural fracture in Figure 25. This shows that when S=20m there is approximately a 5% reduction after 500 days, but after 1,000 days there is almost no

Journal Pre-proof

reduction. For S=10 m and S=5m, respectively 10% and 27% reductions are observed. This suggests that correctly defining the fracture spacing is critical to accurately model gas production from hydraulically fractured reservoirs.

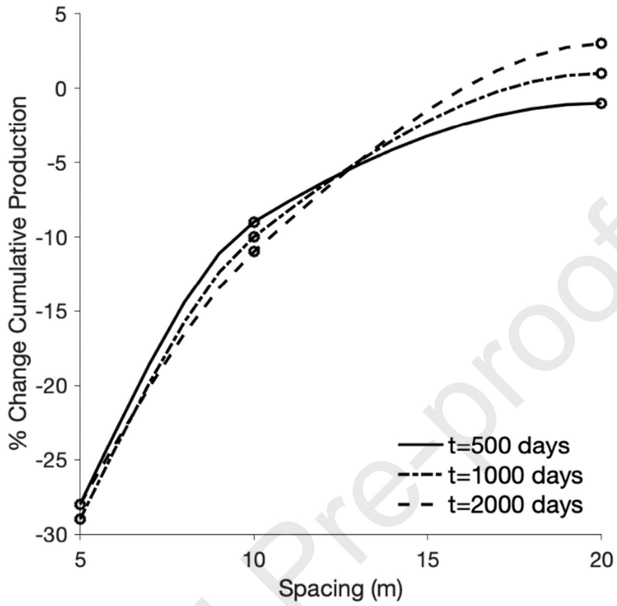


*Figure 25- Percentage change in cumulative production compared to the case with no natural fracture present*

**3.3.4 In-Situ Stresses**

When horizontal in-situ stresses are relatively isotropic, natural fractures and pre-existing planes of weakness have high potential to initiate and propagate hydraulic fractures. However, when the differential stress is high the least energy configuration may still be orientated along the maximum principal stress instead of along pre-existing planes of weakness. Therefore, the propagation of hydraulic fractures will be heavily influenced by in-situ stresses. The FUM can be applied to shale reservoirs with any range of differential stresses. Hence, to investigate the effect of large differential stresses on the gas production from hydraulically fractured reservoirs (in the presence of natural fractures), we increased the maximum stress while keeping the minimum stress at 48,263 kPa. In these cases, a synthetic natural fracture distribution is applied with an angle of 45°, S=10m and L=10m.

Journal Pre-proof

The effect of increasing the maximum horizontal stress on cumulative gas production is shown in Figure 26. Hydraulic fractures propagating along a natural fracture experience a component of the maximum horizontal stress, and therefore a larger maximum horizontal stress increases the force opposing the opening of fractures. This increased opposition to hydraulic fracture propagation results in fracture networks that penetrate less deeply into the formation and lead to a reduced gas recovery.

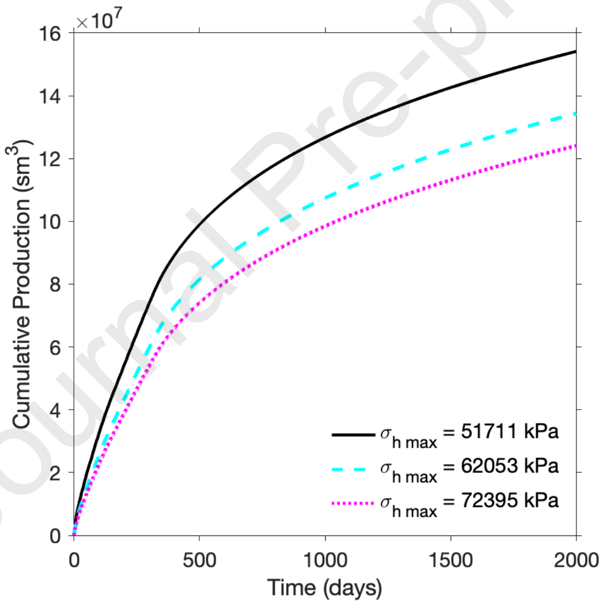


*Figure 26 – Cumulative production with different maximum horizontal stresses with a minimum horizontal stress of 48,263 kPa*

In contrast, the effect of decreasing the minimum horizontal stress is shown in Figure 27 in which a constant maximum stress of 51,200 kPa is used. A decreased minimum horizontal stress makes it easier for fractures to propagate into the formation resulting in fractures that reach a larger volume of the formation. As the mass of proppant used is unchanged, proppant concentration remains very low in parts of this extended fracture network. The fractures extend considerably beyond the region of pressure depletion in Figure 28 (a) but the aperture

Journal Pre-proof

Journal Pre-proof

is so small that they do not contribute towards an increase in permeability. Figure 27 shows that gas production changed slightly by the minimum horizontal stress.

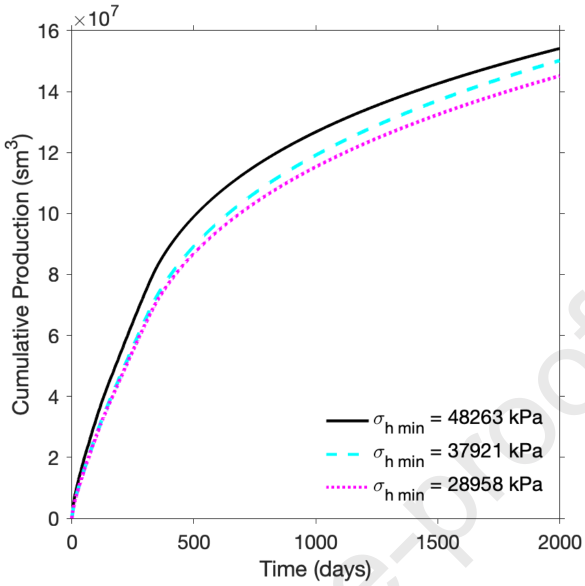


*Figure 27 – Cumulative production with different minimum horizontal stresses with a maximum horizontal stress of 57,711 kPa*

The pressure profiles are shown in Figure 28, demonstrate that when the differential stress is higher, less branching is seen in the fracture network and a smaller area of the reservoir is accessed.

Journal Pre-proof

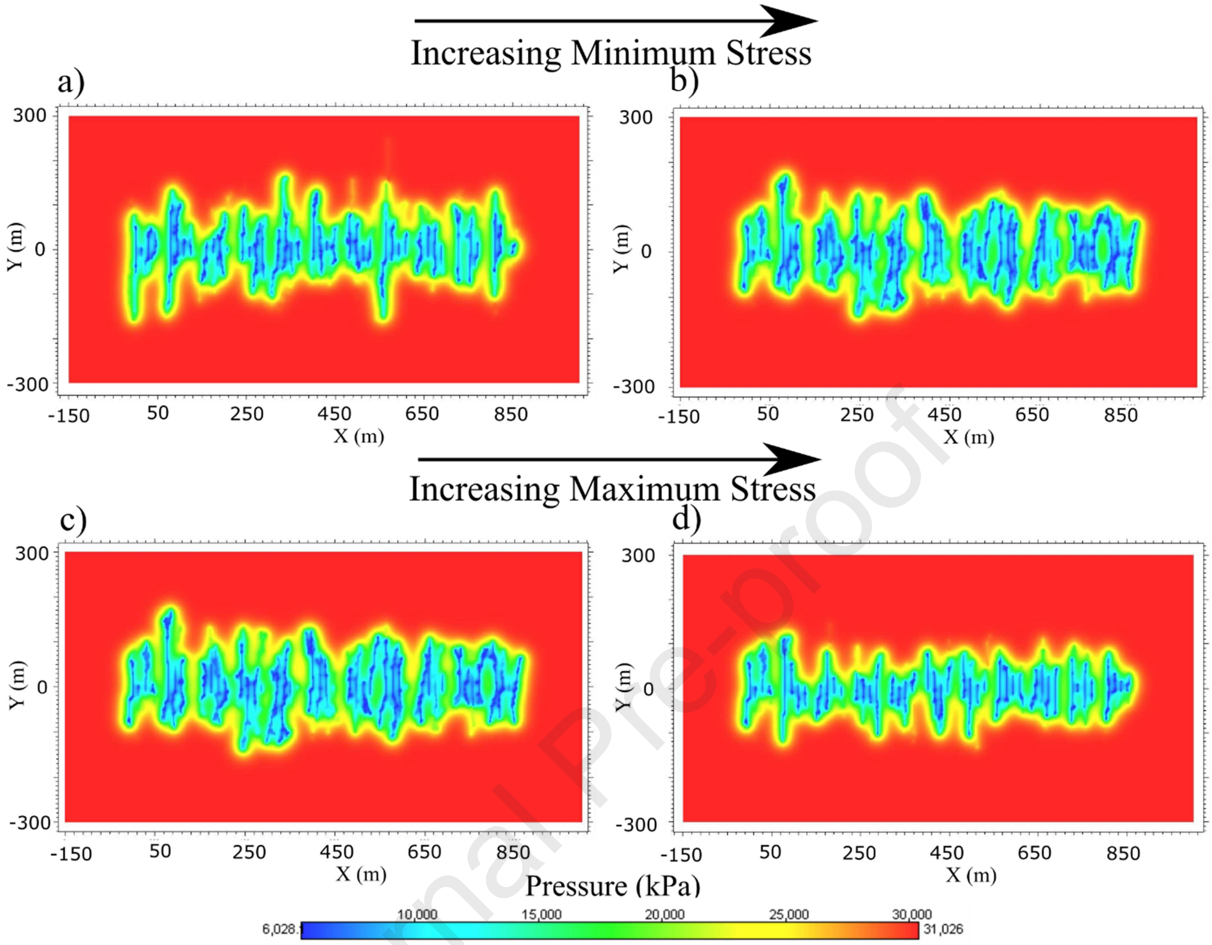


*Figure 28 – Pressure profiles of the reservoir (matrix blocks) after 300 days of production following stimulation of naturally fractured formation with different horizontal stress regimes. a) minimum stress = 28,958 kPa, b) minimum stress = 48,263 kPa both with a maximum stress = 51,711 kPa. c) maximum stress = 51,711 kPa and d) maximum stress = 72,395 kPa both with minimum stress = 48,263 kPa. Cell size 2×2×25m*

Therefore, large differential stresses can either increase or decrease the complexity of fracture networks. In this study, increased maximum stress decreased complexity but also limited the ability of hydraulic fractures to propagate into the formation, leading to a reduced gas recovery. Whereas decreased minimum stress had limited impact.

There are other factors that have not been investigated in this study and may be investigated in the future. If the fracture toughness is very low, which is a characteristic of poorly cemented or open natural fractures, then propagating hydraulic fractures find it very easy to propagate along these natural fractures. This means that regardless of the orientation of the natural fractures the hydraulic fractures are likely to propagate along them. Also, natural fractures may contribute to the total flow from the reservoir which can affect the ultimate recovery factor. Therefore, to predict the production using hydraulic fractures in a naturally fractured shale/tight reservoir, properties of natural fractures and reservoir geomechanics should be coupled.

**3.4 3D Complex Model**

This study has demonstrated the ability of FUM to represent simple fracture segments, real field cases and complex fracture networks formed by the interaction between hydraulic fractures and natural fractures in a finite difference grid. However, this has only been demonstrated using single layer grids. Although the fracture is considered using a 3D geometry, some aspects of this complexity are lost during the upscaling process, and the full complexity FUM can handle is not demonstrated. FUM can also be used with more complex multi-layered 3D grids which allow the upscaled grid to capture more of the complex geometry. A complex, multi-layered fracture distribution is shown in Figure 29 and the complex single fracture stage is shown in Figure 30. This shows the ability to incorporate a more complex distribution of in-situ reservoir properties, such as permeability, which is more typical of a real formation and can be easily loaded into the FUM from an exported static model. Using a multi-layer model, the dip of fractures can also be captured by the FUM. However, in this study only vertical fractures were tested.

Journal Pre-proof

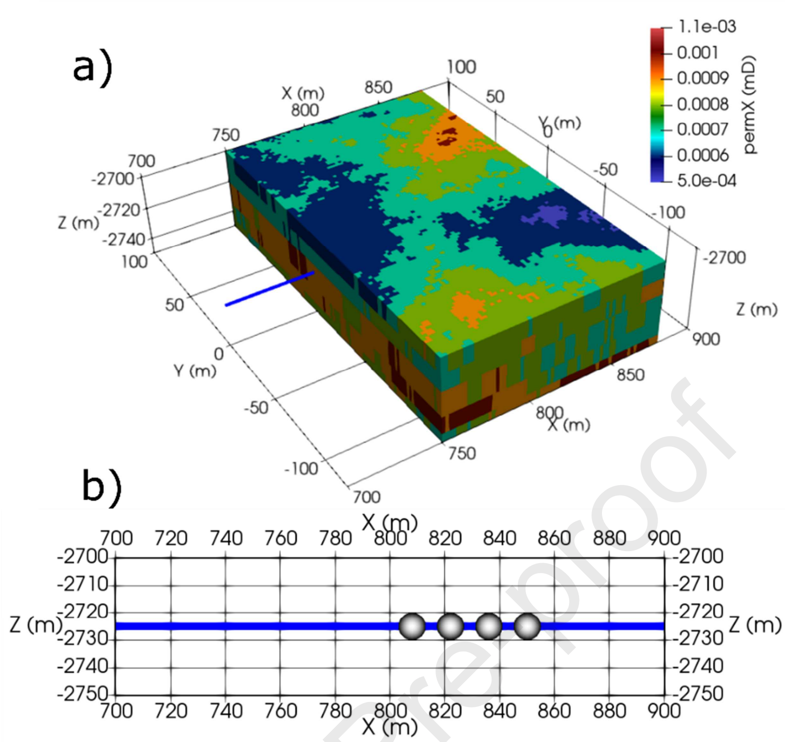


*Figure 29 – a) Unstimulated reservoir permeability distribution to test a highly complex, heterogeneous reservoir with FUM. b) Well trajectory is shown as the blue line, and grey spheres represent perforation clusters*

A well is located parallel to the x-direction at y = 0 m and z = -2,725 m of the model. There are 4 perforation clusters along the well, highlighted in Figure 29 (b), resulting in four fractures branching out from the well into complex fracture segments. Figure 30 (a) shows the fracture surfaces of the reservoir which are produced by an unconventional fracture modelling software (FEM) above the finite difference grid, clipped to -2,725 m and below to expose the top half of the pseudo-fracture system. This complex geometry is captured by the pseudo-fracture network (cells which contain the fracture network) shown in Figure 30 (b). Because a multi layered grid is used, this image shows the 3D ability of the pseudo-fracture system to represent the DFN which was not demonstrated previously. Finally, the pseudo-fracture system with upscaled permeability is shown in Figure 31. This presents the ability of FUM to capture complexities observed in real fields which cannot be captured by other

Journal Pre-proof

simulators. Complex variations of reservoir properties such as Young's Modulus may have a major impact on fracture propagation and by using FUM the effect on production can also be quantified.

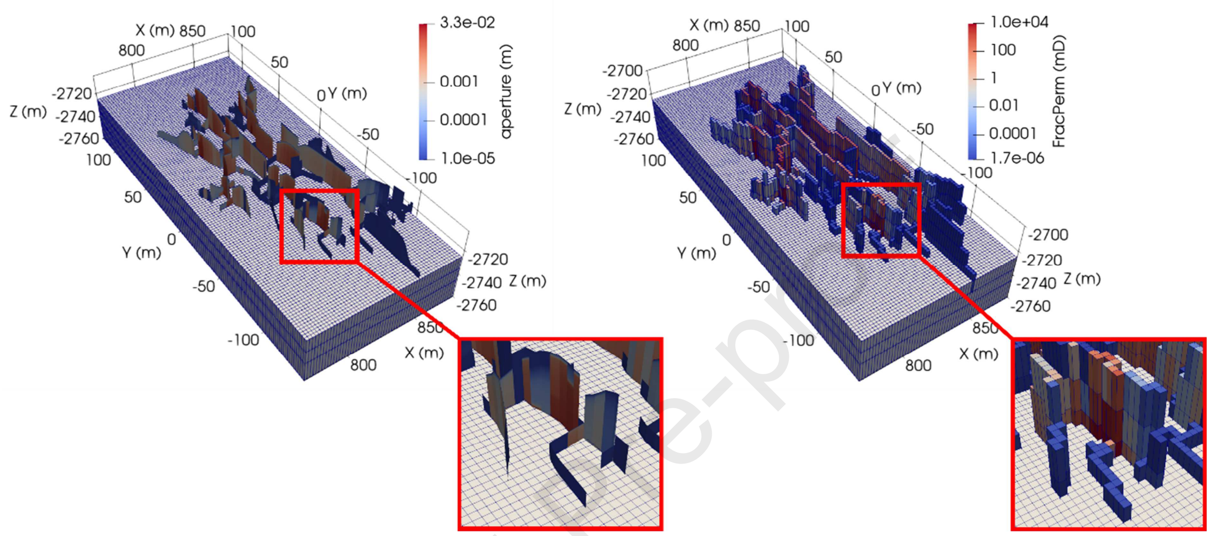


*Figure 30 - a) Fracture surfaces exported from DFN simulation b) Pseudo-fracture network showing the contained fracture permeability created by FUM. Displayed above the finite-difference grid clipped to z=-2725m and below.*

Journal Pre-proof

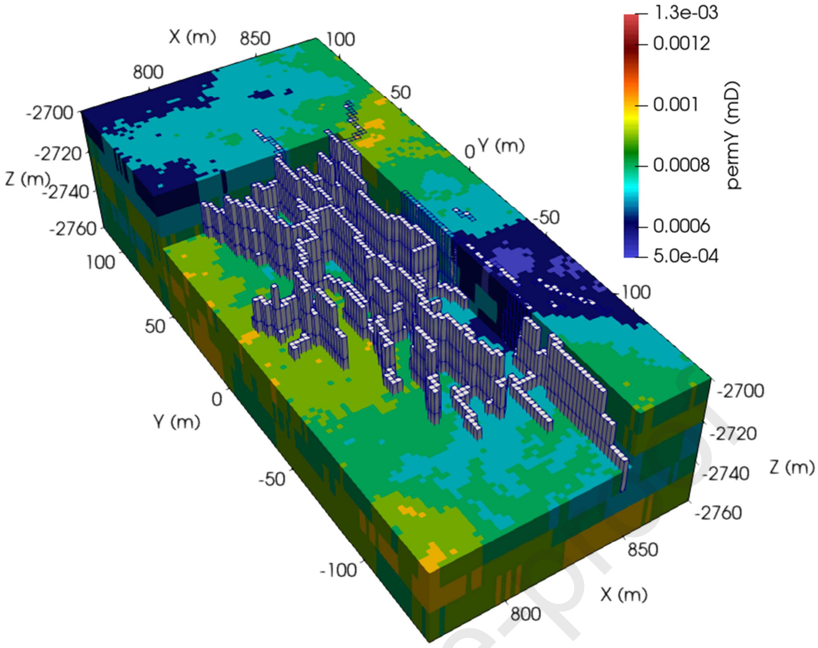


*Figure 31 – Pseudo-fracture network created by FUM in a cut-out section of the finite difference simulation grid. The properties of the pseudo-fracture network are not shown.*

## 4. Conclusions

A fracture upscaling method (FUM) for representing complex fracture networks in a conventional discrete computational grid is presented. The complex hydraulic fracture networks produced by a finite element approach are represented in multiphase flow simulators by using pseudo-fractures. The output models from the FUM are used to estimate production estimations from hydraulically fractured reservoirs using conventional simulators. The key outcomes of the FUM and its application on different cases are as follows:

- Using simple fracture segments, FUM can most capture hydraulic fractures with a range of grid cell sizes.
- The upscaling method is used to investigate the effects that natural fractures can have on gas production, in particular the effect of natural fracture angle, length and spacing.

Journal Pre-proof

- The angle between natural fractures and maximum in-situ stress strongly controls the fracture propagation and subsequently there is approximately a 20% difference in cumulative production with all configurations. Recovery is poorest when the angle is 80°.
- Small fracture spacing leads to more complex fracture networks that do not deeply penetrate the formations resulting in poor recovery.
- Fracture length has a relatively limited effect on gas recovery, but small lengths lead to simpler fracture networks that penetrate deeper resulting in a higher recovery.
- When there is a large difference between the horizontal principal stresses there is higher resistance on fractures propagating along natural fractures. As a result, fracture networks are less complex, and the impact on production is reduced.
- FUM is demonstrated to capture more realistic distributions of reservoir properties in addition to complex 3D fracture geometry.
- To fully understand the impact of natural fractures on gas production in hydraulically fractured reservoirs, their properties and reservoir geomechanics need to be coupled, to investigate whether they may have positive or negative effect on production.

## 5. Acknowledgments

The authors would like to thank the School of Engineering at the University of Aberdeen for financial support and providing the required facilities to complete the study. Support from Computer Modelling Group and Schlumberger for the use of their software packages is greatly acknowledged. This research did not receive any specific grant from funding agencies in the public, commercial, or not-for-profit sectors.

Journal Pre-proof

# 6. References


Arri, L.E., Yee, D., Morgan, W.D. and Jeansonne, M.W., 1992. “Modeling Coalbed Methane Production With Binary Gas Sorption”, Presented at the SPE Rocky Mountain regional meeting, Casper, Wyoming 18-21 May, SPE-2463-MS

Burnham, A., Han, J., Clark, C.E., Wang, M., Dunn, J.B. & Palou-Rivera, I. 2012, "Life-Cycle Greenhouse Gas Emissions of Shale Gas, Natural Gas, Coal, and Petroleum", *Environmental science & technology,* vol. 46, no. 2, pp. 619-627.

Daigle, H., Ezidiegwu, S. and Turner, R., 2015. "Determining Relative Permeability In Shales By Including The Effects Of Pore Structure On Unsaturated Diffusion And Advection", Presented at the SPE Annual Technical Conference and Exhibition, Houston, Texas, 28-30 September, SPE-175019-MS

Dahi-Taleghani, A. & Olson, J.E. 2013, "How Natural Fractures Could Affect Hydraulic-Fracture Geometry", *SPE Journal,* vol. 19, no. 01, pp. 161-171.

Dahi-Taleghani, A. & Olson, J.E. 2011, "Numerical Modeling of Multistranded-Hydraulic-Fracture Propagation: Accounting for the Interaction Between Induced and Natural Fractures", *SPE Journal,* vol. 16, no. 03, pp. 575-581.

Daniels, J.L., Waters, G.A., Le Calvez, J.H., Bentley, D. & Lassek, J.T. 2007, "Contacting More of the Barnett Shale Through an Integration of Real-Time Microseismic Monitoring, Petrophysics, and Hydraulic Fracture Design", Presented at the SPE Annual Technical Conference and Exhibition, Anaheim, California, 11-14 November, SPE-110562-MS.

Egboga, N.U., Mohanty, K.K. & Balhoff, M.T. 2017, "A feasibility study of thermal stimulation in unconventional shale reservoirs", *Journal of Petroleum Science and Engineering,* vol. 154, pp. 576-588.

EIA 2019, 31/07/2019-last update, *U.S. Energy Information Administration* [Homepage of U.S. Energy Information Administration], [Online]. Available: https://www.eia.gov [2019, 08/14].

EIA 2018, 31/12/18-last update, *Natural Gas Gross Withdrawals and Production* [Homepage of US Energy Information Agency], [Online]. Available: https://www.eia.gov/dnav/ng/ng_prod_sum_dc_NUS_mmcf_a.htm [2019, 22/01/18].

Evans, R.D. and Civan, F., 1994. Characterization of Non-Darcy Multiphase Flow in Petroleum Bearing Formations. Report, US DOE. Contract No. DE-AC22-90BC14659. School of Petroleum and Geological Engineering, University of Oklahoma.

Forchheimer, P., 1901. Wasserbewegung durch Boden. Z. Ver. Deutsch. Ing, 45, pp. 1782-1788.

Godec, M., Koperna, G., Petrusak, R. & Oudinot, A. 2013, "Potential for enhanced gas recovery and CO2 storage in the Marcellus Shale in the Eastern United States", *International Journal of Coal Geology,* vol. 118, pp. 95-104.

Hall, F.E., Chunhe, Z., Gasem, K.A.M., Robinson, R.L. and Dan, Y., 1994, "Adsorption of Pure Methane, Nitrogen, and Carbon Dioxide and Their Binary Mixtures on Wet Fruitland Coal", Presented at the SPE Eastern Regional Meeting, Charleston, West Virginia 8-10 November, SPE-29194-MS

Kresse, O., Cohen, C., Weng, X., Wu, R. & Gu, H. 2012, "*Numerical Modeling of Hydraulic Fracturing In Naturally Fractured Formations"*, Presented at the 46th US Rock Mechanics/Geomechanics Symposium, Chicago, Illinois, 24-27 June, ARMA-2012-292

Kresse, O., Weng, X., Gu, H. & Wu, R. 2013, "Numerical Modeling of Hydraulic Fractures Interaction in Complex Naturally Fractured Formations", *Rock Mechanics and Rock Engineering,* vol. 46, no. 3, pp. 555-568.

Letham, E.A. and Bustin, R.M., 2015, "Klinkenberg gas slippage measurements as a means for shale pore structure characterization", *Geofluids*, vol. 16 no. 2, pp. 264-278.

Lei, Q., Latham, J. & Tsang, C. 2017, "The use of discrete fracture networks for modelling coupled geomechanical and hydrological behaviour of fractured rocks", *Computers and Geotechnics,* vol. 85, pp. 151-176.

Liang, F., Ryvak, M., Sayeed, S. & Zhao, N. 2012, "The role of natural gas as a primary fuel in the near future, including comparisons of acquisition, transmission and waste handling costs of as with competitive alternatives", *Chemistry Central Journal,* vol. 6, no. 1, pp. 1-24.

Liu, L., Li, L., Elsworth, D., Zhi, S. & Yu, Y. 2018, "The Impact of Oriented Perforations on Fracture Propagation and Complexity in Hydraulic Fracturing", *Processes,* vol. 6, no. 11.

Luo, W., Tang, C. and Zhou, Y. 2019, "A New Fracture-Unit Model and Its Application to a Z-Fold Fracture". SPE Journal, vol. 24 no. 01, pp. 319-333.

Moinfar, A., Varavei, A., Sepehrnoori, K. & Johns, R.T. 2014, "Development of an Efficient Embedded Discrete Fracture Model for 3D Compositional Reservoir Simulation in Fractured Reservoirs", *SPE Journal,* vol. 19, no. 02, pp. 289-303.

Moreno, J., Tarrahi, M., Gildin, E. & Gonzales, S. 2014, "*Real-Time Estimation of Hydraulic Fracture Characteristics From Production Data"*, Presented at the SPE/AAPG/SEG Unconventional Resources Technology Conference, Denver, Colorado, 25-27 August, URTEC-1923687

Nassir, M., Settari, A. & Wan, R. 2014, "Prediction Of SRV And Optimization Of Fracturing In Tight Gas And Shale Using a Fully Elasto-plastic Coupled Geomechanical Model", *SPE Journal,* vol. 19, no. 5, pp. 771-785.

Journal Pre-proof

Nassir, M., Settari, A. & Wan, R.G. 2010, *"Modeling Shear Dominated Hydraulic Fracturing as a coupled fluid-solid interaction"*, Presented at the International Oil and Gas Conference and Exhibition, Beijing, China, 8-10 June, SPE-131736-MS.

Ren, L., Lin, R., Zhao, J., Rasouli, V., Zhao, J. & Yang, H. 2018, "Stimulated reservoir volume estimation for shale gas fracturing: Mechanism and modeling approach", *Journal of Petroleum Science and Engineering*, vol. 166, pp. 290-304.

Roussel, N.P. & Sharma, M.M. 2011, "Strategies to Minimize Frac Spacing And Stimulate Natural Fractures in Horizontal Completions", Presented at the SPE Annual Technical Conference and Exhibition, Denver, Colorado, 30 October-2 November, SPE-146104-MS.

Sakhaee-Pour, A. & Wheeler, M.F. 2016, "Effective Flow Properties for Cells Containing Fractures of Arbitrary Geometry", *SPE Journal*, vol. 21, no. 03, pp. 965-980.

Sharifi Haddad, A., Hassanzadeh, H. and Abedi, J. 2012. "Advective–diffusive mass transfer in fractured porous media with variable rock matrix block size". *Journal of Contaminant Hydrology*, **133**, pp. 94-107.

Sharifi Haddad, A., Hassanzadeh, H., Abedi, J. and Chen, Z. 2013. "Lumped mass transfer coefficient for divergent radial solute transport in fractured aquifers. *Journal of Hydrology*, vol. 495, pp. 113-120.

Sharifi Haddad, A., Hassanzadeh, H., Abedi, J., Chen, Z. & Ware, A. 2015, "Characterization of Scale-Dependent Dispersivity in Fractured Formations Through a Divergent Flow Tracer Test", *Groundwater*, vol. 53, pp. 149-155.

Sharifi Haddad, A., Hejazi, S.H. and Gates, I.D., 2017. "Modeling solvent enhanced gravity drainage from a single matrix block in fractured oil reservoirs", *Journal of Petroleum Science and Engineering*, vol. 152, pp. 555-563.

Sherratt, J., Sharifi Haddad, A. and Rafati, R. 2018. "Hot Solvent-Assisted Gravity Drainage in Naturally Fractured Heavy Oil Reservoirs: A New Model and Approach to Determine Optimal Solvent Injection Temperature". *Industrial & Engineering Chemistry Research*, vol. 57 no. 08, pp. 3043-3058.

U.S. Department of Energy 2018, *U.S. Crude Oil and Natural Gas Proved Reserves, Year-end 2016*, U.S. Department of Energy.

Wan, X., Rasouli, V., Damjanax, B., Yu, W., Xie, H., Li, N., Rabiel, M., Miao, J. and Liu, M. 2020 "Coupling of fracture model with reservoir simulation to simulate shale gas production with complex fractures and nanopores". Journal of Petroleum Science and Engineering, vol. 193, pp. 107422.

Witherspoon, P.A., Wang, J.S.Y., Iwai, K. & Gale, J.E. 1980, "Validity of Cubic Law for fluid flow in a deformable rock fracture", *Water Resources Research*, vol. 16, no. 6, pp. 1016-1024.

Journal Pre-proof

Journal Pre-proof

Wu, K. & Olson, J.E. 2015, "Numerical Investigation of Complex Hydraulic Fracture Development in Naturally Fractured Reservoirs", Presented at the SPE Hydraulic Fracturing Technology Conference, The Woodlands, Texas, 3-5 February, SPE-173326-MS

Yu, W., Hu, X., Wu, K., Sepehrnoori, K. & Olson, J.E. 2017, "Coupled Fracture-Propagation and Semianalytical Models to Optimize Shale Gas Production", *SPE Reservoir Evaluation & Engineering,* vol. 20, no. 04, pp. 1004-1019.

Zhang, F., & Emami-Meybodi, H. 2020, "A semianalytical method for two-phase flowback rate-transient analysis in shale gas reservoirs". *SPE Journal, vol. 25* no. 04, pp. 1599-1622.

Zhou, L., Su, X., Lu, Y., Ge, Z., Zhang, Z. & Shen, Z. 2019, "A New Three-Dimensional Numerical Model Based on the Equivalent Continuum Method to Simulate Hydraulic Fracture Propagation in an Underground Coal Mine", *Rock Mechanics and Rock Engineering*, vol. 52, no. 8, pp. 2871-2887.

Journal Pre-proof

Journal Pre-proof

**Highlights:**

- A Fracture Upscaling Model (FUM) presented to model complex fracture geometries
- FUM translates the output of any DFM for using by any FD-based reservoir simulator
- Natural fractures introduce complex fracking patterns that can be captured by FUM
- FUM is tested against gas production data from a hydraulically fractured well

Journal Pre-proof

**Declaration of interests: none**

☒ The authors declare that they have no known competing financial interests or personal relationships that could have appeared to influence the work reported in this paper.

☐The authors declare the following financial interests/personal relationships which may be considered as potential competing interests:

| Declarations of interest: none |
| --- |

Journal Pre-proof